

COMPARATIVE PROTEIN ANALYSIS OF TWO HUMAN ISOFORMS  
CENTRIN 1 AND CENTRIN 2

by  
Myrna Reyes Blas

A thesis submitted in partial fulfillment of the requirements for the degree of

MASTER OF SCIENCE  
in  
CHEMISTRY

UNIVERSITY OF PUERTO RICO  
MAYAGÜEZ CAMPUS  
2008

Approved by:

---

Marisol Vera, Ph.D.  
Member, Graduate Committee

---

Date

---

Gustavo López, Ph.D.  
Member, Graduate Committee

---

Date

---

Belinda Pastrana - Ríos, Ph.D.  
President, Graduate Committee

---

Date

---

Aldo Acevedo, Ph.D.  
Representative of Graduate Studies

---

Date

---

Francis Patron, Ph.D.  
Chairperson of the Department

---

Date

## ABSTRACT

Centrin is a calcium binding protein belonging to EF-hand superfamily that is found only in eukaryotic cells from yeast to humans. Three isoforms have been identified in humans two of which are presented in this work: human centrin 1 (Hcen1) and human centrin 2 (Hcen2). Both are comprised of 172 amino acids having between them more than 80 % sequence identity. Hcen1 are localized in the central lumen of the basal bodies of the sperm and Hcen2 are mainly within centrioles. In order to know more about the structure, dynamics and relative stability we, have performed Hcen1 and Hcen2 bacterial expression, isolation, and purification; for their biophysical characterization using FT-IR spectroscopy and two dimensional correlation spectroscopy analysis. The order of events throughout the thermal perturbation was established from 1700 – 1530  $\text{cm}^{-1}$  spectral region study. The thermal stability for Hcen1 is described as the follows:  $\alpha$ -helix <  $\beta$ -sheets < glutamate <  $\beta$ -turns, while for Hcen2 the thermal stability is the following: arginine <  $3_{10}$ -helix < aspartate/glutamate < random coil <  $\alpha$ -helix < aggregation < loops.

A higher thermal stability was observed for Hcen1 than for Hcen2 and a pretransition at 1.7 – 4.8 °C and the onset of the transition temperature was also observed for Hcen1 at 80.5 – 84 °C. Unlike Hcen1, Hcen2 was observed to aggregate at the temperature range of 43 – 58 °C. Therefore, we were able to establish differences in stability, conformation and dynamics between these isoforms.

## RESUMEN

Centrin es una proteína enlazante de calcio perteneciente a la superfamilia de proteínas de mano EF que se encuentra solamente en células eucariotas desde levaduras hasta células humanas. De las tres isoformas que han sido identificadas en humanos, dos son presentadas en este trabajo: centrin humana 1 (Hcen1) y centrin humana 2 (Hcen2). Ambas tienen una secuencia de 172 amino ácidos con un 80% de identidad entre ellas. Hcen1 está localizada en el lumen central de los cuerpos basales del espermatozoide y Hcen2 se encuentra principalmente en los centriolos. En el interés de conocer más acerca de su estructura, dinámica y estabilidad relativa, hemos realizado la expresión bacteriana, aislamiento y purificación para su caracterización biofísica usando espectroscopia de infrarrojo con transformada de Fourier (FT-IR), así como el análisis espectroscópico de correlación bidimensional. El orden de los eventos durante la perturbación termal fué establecido analizando la región espectral  $1700 - 1530 \text{ cm}^{-1}$ . La estabilidad termal para Hcen1 es descrita como la siguiente:  $\alpha$ -hélice < hojas  $\beta$  < glutamato < vueltas  $\beta$ , mientras que para Hcen2 la estabilidad termal es la siguiente: arginina < hélice  $3_{10}$  < aspartato/glutamato < estructura desordenada < hélice  $\alpha$  < agregación < giros.

Una mayor estabilidad termal fue observada para Hcen1 con una pre-transición entre  $1.7 - 4.8 \text{ }^\circ\text{C}$  así como un inicio de temperatura de transición entre  $80.5 - 84 \text{ }^\circ\text{C}$ . A diferencia de Hcen1, en Hcen2 fué observada la agregación dentro del rango de temperatura de  $43 - 58 \text{ }^\circ\text{C}$ . De acuerdo con estos resultados, fué posible establecer diferencias en la estabilidad, conformación y dinámica, entre estas isoformas.

## *Dedication*

*To **GOD** because.... “You saw me before I was born. Every day of my life was recorded in your book. Every moment was laid out before a single day had passed”. (Psalm 139:16)”*

*To **Anibal**; my husband; for stimulating, supporting and loving me.*

*To **Anibal E.** and **Jamefy**; my children, because they have motivated me to be an example for them.*

*To my **parents**... for their affection; and because through the distance they have become my unconditional support.*

## ACKNOWLEDGEMENTS

I want to express my deepest appreciation to Dr. Belinda Pastrana for the opportunity to develop this research under her supervision and guidance. She not only taught me science, but also taught me how to embrace and survive the exigencies of life. I wish to thank to my graduate committee, Dr. Marisol Vera and Dr. Gustavo Lopez, for their recommendations.

My deepest gratitude goes to the Chemistry Department for accepting me as a graduate student and providing financial support.

I would like to acknowledge the NIH-MBRS-SCORE Grant, SO6GM08103 and NIH-Center of Biomedical Research Excellence (COBRE II) 1P20RR16439-01 for providing the funds and resources toward the development of this research.

To my friends at the lab, who did not only helped, taught, supported, and stimulated me during this work, but also offered me their friendship: Lilix (you know how much), Daniel, Zuleika, Anamaria, Sindy, Jessica, Verónica and Ibon.

I want to acknowledge Anibal and Lucy, my mother and father-in-law, for caring for my family in such a loving way when I could not do it.

To Anibal, my beloved husband, for his patience, unconditional support and for being there as I needed to vent.

To Estela and Enrique, my parents for setting the foundation of whom I am today, encouraging me even from a distance, and saying: “Echele ganas mija”.

## Table of Contents

Table of Contents.....	vi
List of Tables.....	viii
List of Figures.....	ix
CHAPTER I.....	2
JUSTIFICATION.....	2
OBJECTIVES.....	4
CHAPTER II.....	5
LITERATURE REVIEW.....	5
Cell Cycle and the Centrosome.....	5
Centrin a Calcium-binding Protein.....	11
Structural Studies of Centrin.....	18
<i>X-Ray diffraction crystallography</i> .....	18
<i>Nuclear Magnetic Resonance (NMR)</i> .....	23
<i>Fourier-Transform Infrared (FT-IR) Spectroscopy</i> .....	27
Infrared spectroscopy.....	28
<i>Hydrogen / deuterium exchange of the protein sample</i> .....	34
Two-Dimensional Correlation Spectroscopy.....	38
CHAPTER III.....	45
MATERIALS AND METHODS.....	45
Bacterial expression of Human centrin 1 and 2.....	45
Isolation and Purification of Human centrin 1 and 2.....	46
FT-IR Spectroscopy.....	48
Data Analysis.....	49
CHAPTER IV.....	50
RESULTS AND DISCUSSIONS.....	50
Bacterial expression of Human centrin 1 and 2.....	50

Isolation and Purification of Human centrin 1 and 2 .....	56
<i>Affinity Chromatography using Phenyl Sepharose CL-4B column</i> .....	56
<i>Anion Exchange Chromatography</i> .....	61
<i>UV Spectroscopy Assays</i> .....	64
<i>Mass Spectrometry</i> .....	65
FT-IR Spectroscopy.....	69
Curve-fitting analysis .....	73
Two-dimensional correlation analysis .....	76
<i>Synchronous plots</i> .....	76
<i>Asynchronous plots</i> .....	77
Thermal dependence study .....	82
Two-dimensional correlation analysis: a detailed description of temperature induced changes in Hcen2.....	84
CHAPTER V .....	92
CONCLUSIONS .....	92
CHAPTER VI.....	94
FUTURE WORKS .....	94
REFERENCES.....	95

## List of Tables

Table 1. Characteristic IR amide bands of the peptide linkage, based in the spectrum of <i>N</i> -methylacetamide.....	31
Table 2. Assignment of amide I/I' band positions to secondary structure.....	36
Table 3. Position of amino acid side chains IR bands present in the Amide I/I' region. ....	37
Table 4. Summary of the percent secondary structure for Hcen1 and Hcen2 .....	74
Table 5. Summary of peak assignment obtained from synchronous and asynchronous plots for Human centrin 1 and Human centrin 2.....	79
Table 6. Summary of phase analysis of the asynchronous plot used to determine the order of events during thermal perturbation for: Hcen1 and Hcen2. ....	81
Table 7. Summary of peak assignment obtained from synchronous and asynchronous plots for each data set from Hcen2 thermal dependence study.....	87
Table 8. Summary of phase analysis of the asynchronous plots used to determine dynamics during the thermal dependence study of Hcen2. ....	88

## List of Figures

Figure 1. Cell and centrosome cycle.....	6
Figure 2. Structure of the centrosome. ....	10
Figure 3. Human centrin and calmodulin homology.....	13
Figure 4. EF-hand motif and calcium coordination:.....	16
Figure 5. Centrin amino acid sequence comparison.....	17
Figure 6. Human centrin 2 and human XPC structure. ....	20
Figure 7. Structure of the Cdc31-Sfi1p complex. ....	22
Figure 8. Working model of the protein multimeric assembly including centrin and Sfi1 in the contractile fibres of the basal bodies. ....	26
Figure 9. <i>N</i> -methylacetamide and peptide bond similarity.....	30
Figure 10. Different components of the amide I band. ....	32
Figure 11. General scheme for obtaining 2D correlational plots ....	41
Figure 12. Schematic synchronous contour plot of a hypothetical two-dimensional correlation analysis. ....	43
Figure 13. Schematic of an asynchronous contour plot using a hypothetical two-dimensional correlation analysis. ....	44
Figure 14. Hcen 1 growth curve plot.....	52
Figure 15. SDS-P Hcen 1 high level expression. ....	53
Figure 16. Hcen 1 growth curve plot.....	54

Figure 17. SDS-PAGE Hcen 2 high level expression.....	55
Figure 18. Phenyl Sepharose chromatogram .....	58
Figure 19. Lab chip electrophoresis gel from Hcen 1 affinity chromatography. ....	59
Figure 20. Lab chip electrophoresis gel from Hcen 2 affinity chromatography. ....	60
Figure 21. Anion exchange chromatogram.....	62
Figure 22. Lab chip electrophoresis gel from Hcen 1 and Hcen 2 anion exchange chromatography.....	63
Figure 23. UV spectrum of pure Hcen1 (similarly for Hcen 2) .....	66
Figure 24. MALDI-TOF MS spectrum of Hcen1.....	67
Figure 25. MALDI-TOF MS spectrum of Hcen2.....	68
Figure 26. FT-IR overlay spectra.....	70
Figure 27. Overlaid difference spectra of Hcen (A) and Hcen2 (B) within spectral region 1700 – 1530 cm <sup>-1</sup> . ....	72
Figure 28. Curve fitted FT-IR spectra of Hcen1 and Hcen2. ....	75
Figure 29. Synchronous and asynchronous contour plots in the spectral region of 1700 – 1530 cm <sup>-1</sup> .....	80
Figure 30. Thermal dependence study for Hcen1(A) and Hcen2 (B) .....	83
Figure 31. Two-dimensional correlation analysis from spectral region 1700 – 1500 cm <sup>-1</sup> for 2 - 16 °C region ( A, C) and 16 - 28 °C region (B, D) ) from Hcen2 thermal dependence study.....	89

Figure 32. Two-dimensional correlation analysis from spectral region $1700 - 1500 \text{ cm}^{-1}$ for $28 - 43 \text{ }^\circ\text{C}$ region (E, G) and $43 - 58 \text{ }^\circ\text{C}$ region (F, H) from Hcen2 thermal dependence study.....	90
Figure 33. Two-dimensional correlation analysis from spectral region $1700 - 1500 \text{ cm}^{-1}$ for $58 - 77 \text{ }^\circ\text{C}$ region from Hcen2 thermal dependence study. ....	91

# CHAPTER I

## JUSTIFICATION

In the last century, the centrosome was considered as an enigmatic cellular structure because of its uniqueness in its discreet size and structure within the cell and because it lacks a membrane that separates it from the rest of the cytoplasm. Its structure consists of two centrioles in a perpendicular arrangement and pericentriolar material. The centrosome is considered to be responsible for nucleation of microtubule polymerization, anchoring the microtubules to create arrays that separate the chromosome, and duplicating exactly once per each cell cycle [Hinchcliffe, et. al. 2001].

It is now estimated that 150-200 different proteins are contained within the centrosome. However, only 30 proteins have been identified and only a handful of them have known functions. Ten of these 30 proteins have also been identified as having a function within the centriole assembly. These include: centrin,  $\alpha$ -,  $\beta$ -,  $\gamma$ -,  $\epsilon$ -tubulin, Sfi1, dynein, ninein, centriolin, cep170, and cenexin among others. Centrins are proteins closely related to calmodulin (CaM), a well known calcium binding protein within this EF-hand family of proteins. Centrins are highly conserved in eukaryotic cells from yeast to humans. In humans, three isoforms of centrin have been identified, of which we are considering two: human centrin 1 (Hcen1) and human centrin 2 (Hcen2). Hcen1 and Hcen2 are comprised of 172 amino acids having between them more than 80 % sequence identity and are localized in the central lumen of the basal bodies of the sperm and centrioles, respectively.

Hcen1 has been located at the base of the flagellar apparatus in sperm cells in humans and mice [Errabolou, et. al. 1994; Schiebel, et.al. 1995; Baum, et. al. 1986; Levy, 1996]. That way, during the fertilization a gamete fusion occurs where the oocytes lack the centriolar structure (centrosome) and the human spermatozoa has a centriole that is used as template by the zygote for its first division. Therefore, Hcen1 plays an important role in motility of the sperm and during the first division of the zygote [Palermo, et. al. 1997]. Unlike Hcen1, Hcen2 is expressed in all somatic cells and has been shown to be required for separation and duplication of the centrioles in HeLa cultured cells [Salisbury, et. al. 2002]. Failure in this duplication process could have disastrous consequences, such as development of cancer [Salisbury, et. al. 1999; Lingle et. al. 1998; Lingle, et. al. 1999; Lingle et.al. 2002].

In order to know a little more about the structure and dynamics of Hcen1 and Hcen2 proteins, we have used Fourier transform infrared (FT-IR) spectroscopy in this work [Pastrana-Rios, et. al. 2002; Sanoguet, et. al. 2006; Arrondo, et. al. 1999; Pastrana-Rios, et. al. 2001 and Graft, et. al. 1997]. A wealth of information about structure and environment of amino-acid side chains and the protein backbone can be deduced from vibrational modes included in the amide I band which has been extensively studied [Barth, et. al. 2002, Heinz, et. al. 2002]. Also, we have used two-dimensional correlation spectroscopy (2D-COS) to analyze the data. 2D-COS has been broadly used by our laboratory in the study of proteins by spreading the vibrational contributions into a second dimension from amide I band [Ortiz, et. al. 2005; Pastrana-Rios, et. al. 2002; Sanoguet, et. al. 2006; Pastrana-Rios, et. al. 2001;

Noda, et. al. 2000, Iloro, I. and Pastrana-Rios, 2006; Pastrana-Rios, B. 2006; Iloro, I. et. al., 2008].

## **OBJECTIVES**

Our objective is to characterize these two isoforms of centrin (Hcen1 and Hcen2) to understand their structure and thermal stability which is important to their function. For this we performed the:

1. expression and purification of Hcen1 and Hcen2
2. thermal dependence studies using FT-IR spectroscopy
3. data analysis using two-dimensional correlation spectroscopy

## CHAPTER II

### LITERATURE REVIEW

#### Cell Cycle and the Centrosome

Proper cell division requires a precisely ordered sequence of biochemical events that assures every daughter cell a full complement of the molecules required for life. This sequence of events is known as cell cycle and the model of this process is drawn as a circle (Figure 1). The cell cycle is divided in two main parts: interphase and mitosis. The interphase is defined by the absence of cell division; therefore, during the interphase the cell grows and replicates its chromosomes. The interphase encompasses three phases: gap 1 phase ( $G_1$ ), where the cell increases in size, produces RNA and synthesizes protein; synthesis phase (S), in which DNA replication occurs; and gap 2 phase ( $G_2$ ), in which the cell continues growing and producing new proteins in preparation for cell division. Interphase is followed by mitotic phase (M), which includes the overlapping processes of mitosis and cytokinesis. In mitosis, the maternal nuclear envelope breaks down. Details about the centrosome during cell cycle are discussed in the following section. Matching chromosomes are pulled to opposite poles of the cell; each set of daughter chromosomes is surrounded by a newly formed nuclear envelope and cytokinesis pinches the cell in half, producing two daughter cells [Nelson, et. al. 2000] (see Figure 1).

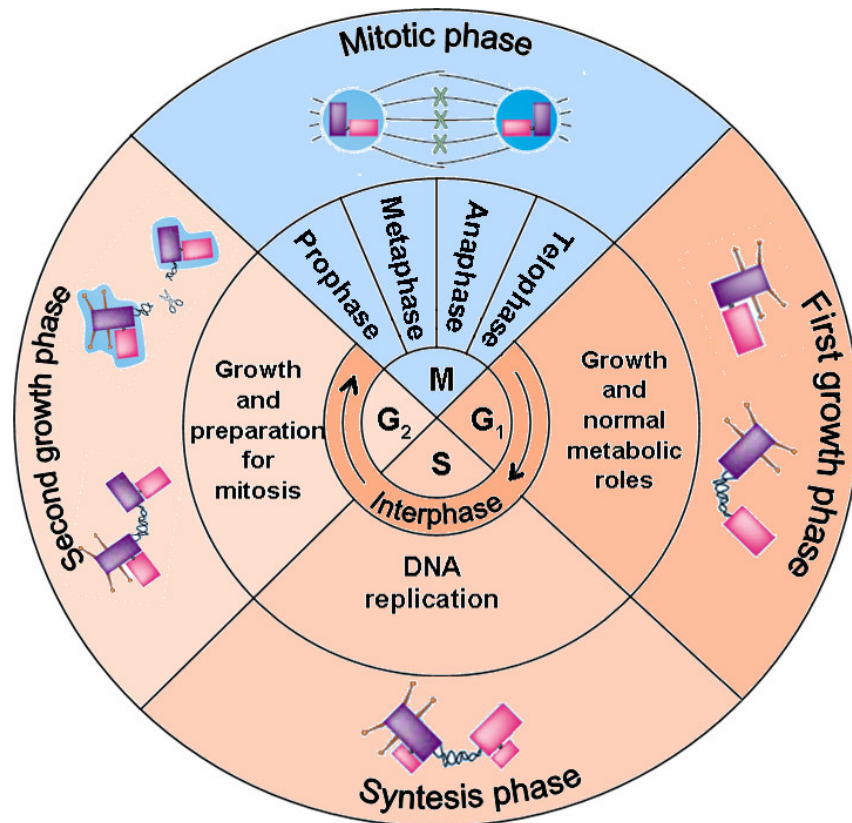


**Figure 1. Cell and centrosome cycle.**

The scheme above describes the different phases of the cell cycle including the mitotic phase. Also shows the centrosome cycle where the centriolar pair is composed of a mature centriole (indicated in purple and carrying appendages) and the immature centriole (pink). The centrioles are likely to be connected via a proteinaceous link (black). G<sub>1</sub>: the centriolar pair consists of one mature and one immature centriole arranged in an orthogonal configuration that is relaxed (disorientation) towards the end of G<sub>1</sub>. S: procentrioles are generated at a right angle to the mother centrioles during S-phase and keep elongating until they achieve their full length in G<sub>2</sub>. G<sub>2</sub>: centriolar linkage disruption between the two parenteral centrioles occurs in late G<sub>2</sub>. G<sub>2</sub>/M: centrosome maturation, involving the acquisition of additional pericentriolar material. Once the cell enters mitosis the two pair of centrioles moves to opposite sides of the nucleus. *Adapted from Solomon, Berg and Martin 2002 and Lange 2002.*

Recent findings have demonstrated that the centrosome is responsible for the regulation of the cell cycle. The centrosome is the only non membranous organelle in most vertebrate cells and it is located near the center of the cell, usually in close proximity to the nucleus. The animal centrosome consists of a pair of centrioles linked together through their proximal regions by a matrix known as the pericentriolar material. This matrix consists of arrangement of 150 - 250 proteins that anchor other matrix components (Figure 2). The centrioles contain cylindrical arrays of triplets microtubules organized with nine-fold radial axis symmetry. The proximal region is structurally similar to the basal bodies of cilia and flagella. In post-mitotic cells, the centrosome contains a mature centriole called the mother centriole (has undergone one cell cycle) and an immature centriole assembled during the previous cell cycle, called the daughter centriole, which is about 80% the length of the mother centriole. The mother centriole is distinguished by two sets of nine appendages at their distal ends, which are thought to be required for anchoring microtubules at the centriole and for docking of centrioles at the plasma membrane during ciliogenesis [Doxsey, et. al. 2001]. In somatic cells, 90% of the stellate fibers are composed by Hcen2, which are located in the distal lumen of both mother and daughter centrioles.

The centrosome plays a major role in organizing the microtubule cytoskeleton in animal cells. During the interphase, the centrosome organizes an astral array of microtubules that is associated with fundamental cellular functions such as intracellular trafficking, cell motility, cell adhesion and cell polarity. The centrosome anchoring capacity requires pericentrosomal satellites. These satellites are composed by PCM1 proteins which bind to centrosome proteins such as centrin, ninein and pericentrin [Salisbury, et. al. 1999].

During the cell cycle the centrosome is also duplicated in phases that include (see Figure 1):

1. ***Centriole splitting or centriole disorientation.*** During late G1 phase the mother-daughter centriole pair is detached and loses the orthogonal relationship. It is not known whether these separated centrioles are still joined by an extensible linkage or have truly split well before the G1-S transition.
2. ***Centriole duplication.*** At the onset of S phase, new centrioles or pro-centrioles are assembled from the sides of the two original centrioles in an orthogonal arrangement. During this time, an early recruitment of centrin in the immediate vicinity of parental centrioles has been observed [La Terra, et. al. 2005]. Centriole duplication and DNA replication are initiated at the same time in the cell cycle.
3. ***Centrosome disjunction.*** Occurs at variable times within G2, the duplicated centrosome disjoints into two functionally separate centrosomes, each containing a mother-daughter pair of centrioles.
4. ***Centrosome separation.*** Occurs prior to the onset of mitosis (this can vary between cells, even those cells in the same population). The sister centrosomes physically separate from each other driven by microtubule motor-mediated sliding of microtubules, and ultimately form the two poles of the mitotic spindle, effectively polarizing the cell.

The requirement of centrin proteins in the centrosome for duplication is not mechanically understood. During fertilization, the oocyte lacks a centriolar structure and the human spermatozoon contributes a centriole to the new zygote [Palermo, et. al. 1997]. The human isoform Hcen1 has been found to be limited to the basal body of the sperm flagella [Errabolou, et. al. 1994], and like Hcen2, Hcen1 participates in centriole duplication only once during the first zygote division and is responsible for the sperm motility [Hart, et. al. 1999].

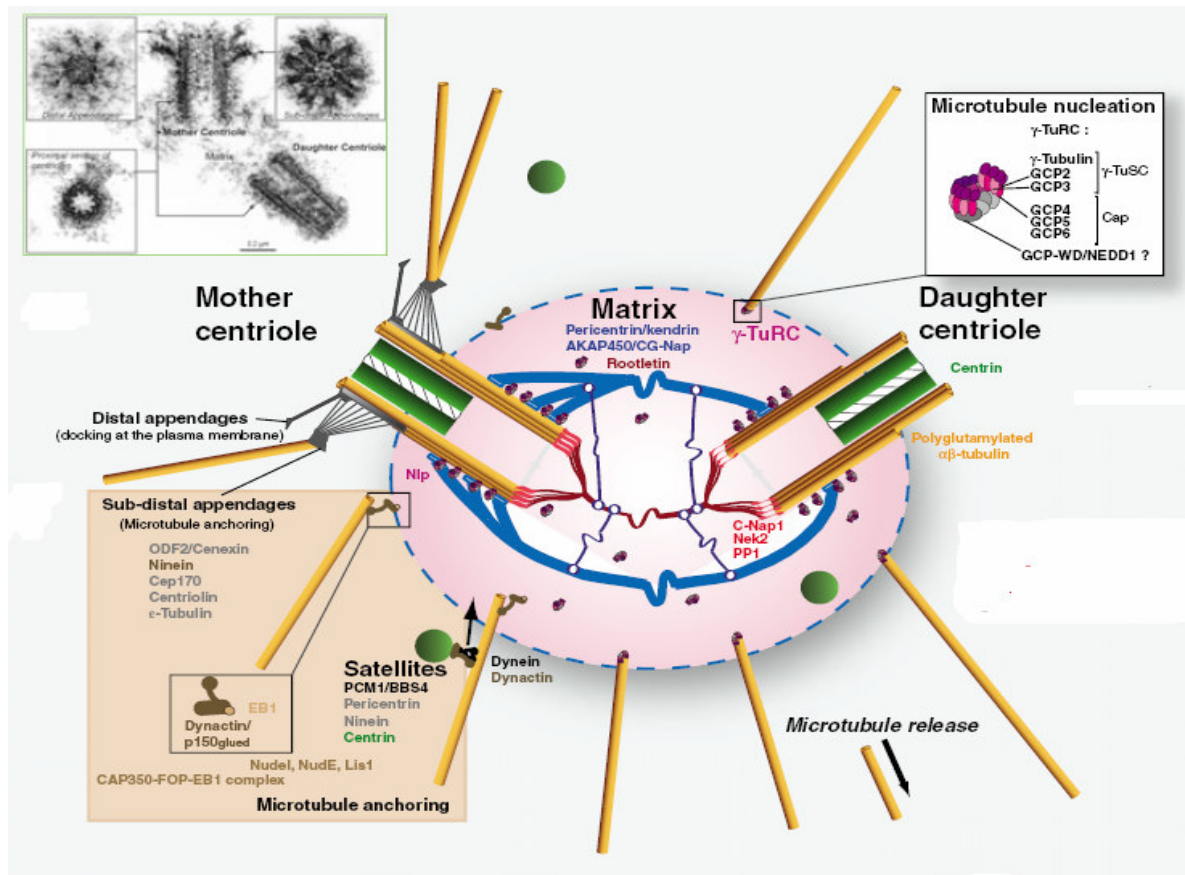


Figure 2. Structure of the centrosome. Modified from Azimzadeh et. al., 2007.

## Centrin, a Calcium-binding Protein

Calcium is a versatile intracellular signal molecule that is able to regulate a large number of cellular functions, including protein synthesis, the cell cycle and apoptosis. The calcium signals inside the cell are analyzed first by special calcium sensor protein, which binds the cation ( $\text{Ca}^{+2}$ ) through a structural and functional motif, known as EF-hand as described first by Kretsinger [Kretsinger, et. al. 1973]. This  $\text{Ca}^{+2}$ -protein complex is now capable of recognizing and binding a target protein. This protein-protein complex is then able to control the target protein's biological activity. A large number of these EF-hand proteins, belonging to the calmodulin super-family, are comprised of two terminal domains which behave as two independent domains [Ortiz, et. al. 2005]. These intern terminal domains are comprised of two EF-hand motifs each [Weber, et. al. 1994].

Centrin is a member of the calcium-binding EF-hand superfamily; an acidic protein of low molecular weight of about 20 kDa. This protein is highly conserved in eukaryotic cells from yeast to humans. Centrin was first discovered in flagellate of a green algae *Tetraselmis striata*, within the basal bodies (the part of the cytoskeleton anchoring the flagella) [Salisbury, et. al. 1984], and associated with the contraction of calcium-sensitive structures including the nuclear basal body connector and the distal striated fibers [Salisbury, et. al. 1995 and Schiebel, et. al. 1995]. See Figure 3.

In humans, there are three isoforms identified to date for centrin (Hcen1, Hcen2, and Hcen3). Studies by immunoelectron microscopy have been used to identify the location of these proteins in central lumen of centrioles of centrosomes and basal bodies. Hcen3 is

exclusively a core component of the basal body centriole; Hcen2 is ubiquitously expressed, whereas Hcen1 expression is restricted to male germ cells [Paoletti, et. al. 1996].

According to their amino acid sequence Hcen1 and Hcen2 are phylogenetically related having 80-90% sequence identity, but are more distant from Hcen3 which has about 55% sequence identity when compared to Hcen1 and Hcen2 (figure 3). Moreover, the sequence of Hcen1 and Hcen2 are closely related to *Chlamydomonas reinhardtii* centrin (CCen) whereas, Hcen3 is related to *Saccharomyces cerevisiae* centrin (Cdc31), strongly suggesting two divergent subfamilies [Wolfrum, et. al. 2002]. While Hcen3, as its yeast relative Cdc31, participates in centrosome duplication, Hcen1 and Hcen2 play a role in centriole separation and duplication preceding centrosome duplication, but the functional mechanism is not known [Lutz, et. al. 2001]. Also, Hcen1 and Hcen2 share about 50% sequence identity with human calmodulin.

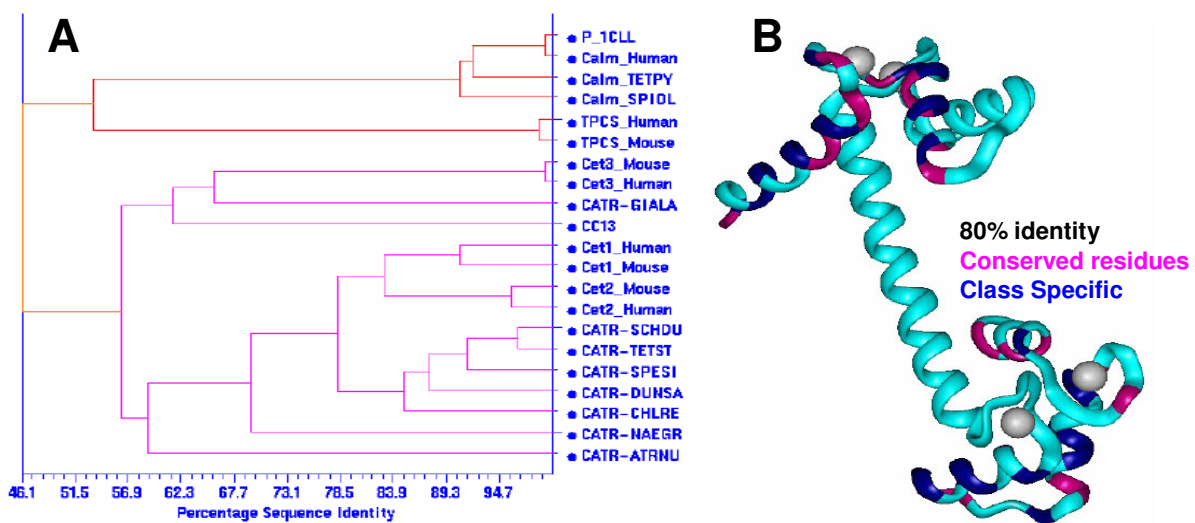


**Figure 3. Human centrin and calmodulin homology.**

(A) Evolutionary trace and (B) structural homology for calmodulin and human centrin generated using BLAST from the National Center of Biotechnology Information (NCBI), Clustal W from European Bioinformatics Institute (EBI), and binding site from Insight II™ of Accelrys.

Structurally, centrin contains four EF-hand consensus motifs (Figure 4a). These regions are the most highly conserved features of the protein as compared to other members of the EF-hand superfamily. The classical EF-hand is a helix-loop-helix motifs characterized by a sequence of, usually, 12 residues with the pattern  $X \cdot Y \cdot Z \cdot -Y \cdot -X \cdot \cdot -Z$ , where, X, Y, Z, -X, -Y and -Z are ligands that participate in metal coordination and the dots represent intervening residues [Lewith-Bentley, et. al. 2000]. Unlike Ccen in which all four EF-hand motifs bind  $Ca^{+2}$ , human isoforms can only bind two  $Ca^{+2}$  ions per protein. The EF-hand motif sequence forms a loop that accommodates  $Ca^{+2}$  through seven ligands at the vertices of pentagonal bipyramid coordination. These ligands are oxygen atoms from three mono-dentate side chains, one backbone carbonyl, one water H-bonded to side chain and one bi-dentate side chain (glutamate) shown in Figure 4b. Hcen1 and Hcen2 have a strong calcium binding site (site IV) and a weaker calcium binding site (site III) in the C-terminal domain. In contrast, Hcen3 and Cdc31 exhibit a mixed  $Ca^{+2}/Mg^{+2}$  binding site located in N-terminal domain [Salisbury, et. al. 1995; Wolfrum, et. al. 2002; Pastrana-Rios, et. al. 2002; Weich, et. al. 1996 and Yang, et. al. 2006a].

The variability in the sequence between Hcen1 and Hcen2 is observed in the amino-terminal domain about 20 amino acids in length from the N-terminal end. This region is comprised of eight hydrophobic and six positively charged residues. The carboxy-terminal domain contains a putative consensus sequence site  $K_{167}KTS^*LY_{172}$  (\* for phosphorylation as reported by Lutz, and the structural and stability consequences reported by Sanoguet and Meyn 2006). Evidence is growing towards a putative kinase known as Aurora A. Furthermore, only the carboxy-terminal domain can bind target peptides (see Figure 5).

Sequence identity is high between Hcen1 and Hcen2 that we are compelled to carry out a comparative study.

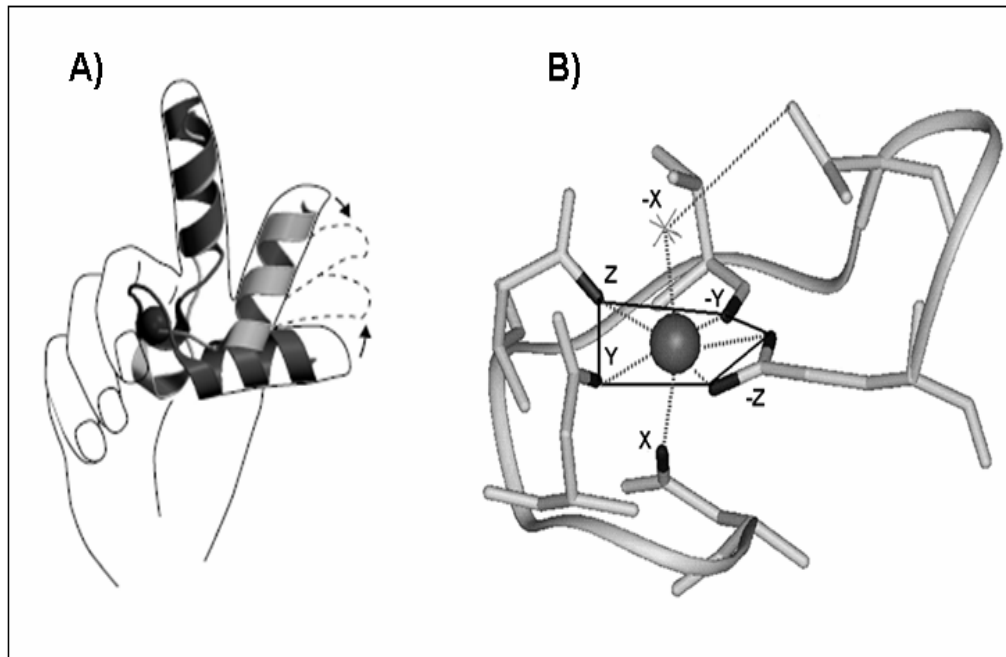


**Figure 4. EF-hand motif and calcium coordination:**

The EF-hand motif. (A) A symbolic representation of the EF-hand motif. Helix E winds down the index finger, whereas helix F winds up the thumb of a right hand. When the calcium ion binds, helix F moves from the closed (apoprotein, light grey) to the open (holoprotein, dark grey) conformation. (B) The geometry of the calcium ligands. At position X and Y, usually are found the side chains of Asp or Asn; the side chains of Asp, Asn or Ser are found in Z and a backbone peptide carbonyl oxygen lies at  $-Y$ .  $-X$  is usually a water molecule and  $-Z$  is a conserved bidentate ligand, Glu or Asp. *Adapted from Lewit-Bentley and Réty 2000*



## Structural Studies of Centrin

### *X-Ray diffraction crystallography*

X-ray diffraction crystallography is at present the reference technique used to determine the complete three dimensional structure of a protein. In principle, the structure can be determined in the absence of any additional information (such as sequence). This technique requires the molecule to form well-ordered crystals but is complicated by not having a clear standardized protocol that simplifies the process. Because each protein has distinct properties in solution, the idea is to crystallize the protein while evaporating the solution and preventing its precipitation or aggregation. Because these proteins are in their solid state, little or no information can be obtained about the dynamic nature of the protein.

### *Hcen2-XPC complex*

Recently, Hcen2 was also found to play a role in the Nucleotide Excision Repair (NER) process by binding to the xeroderma pigmentosum complement protein C (XPC) (Figure 6) [Araki, et. al. 2001; Popescu, et. al. 2003 and Thompson, et. al. 2006]. XPC is involved in recognition of DNA lesions and initiation of global genome nucleotide excision repair. The cooperation of Hcen2 with other proteins like HR23B stimulates XPC NER activity *in vitro* [Popescu, et. al. 2003]. Thompson, et. al. (2006) studied the molecular interaction between Hcen2 and XPC peptide using X-ray diffraction crystallography. They observed that only the carboxy-terminal domain of Hcen2 binds the XPC peptide and two

calcium atoms, while the N-terminal lobe is in a closed conformation causing distortions in the loops of sites I and II abolishing the high affinity for calcium. Also, they observed that two XPC peptides bound to separate Hcen2 molecules interact to form an  $\alpha$ -helical coiled-coil conformation (Figure 6C) [Thompson, et. al. 2006].

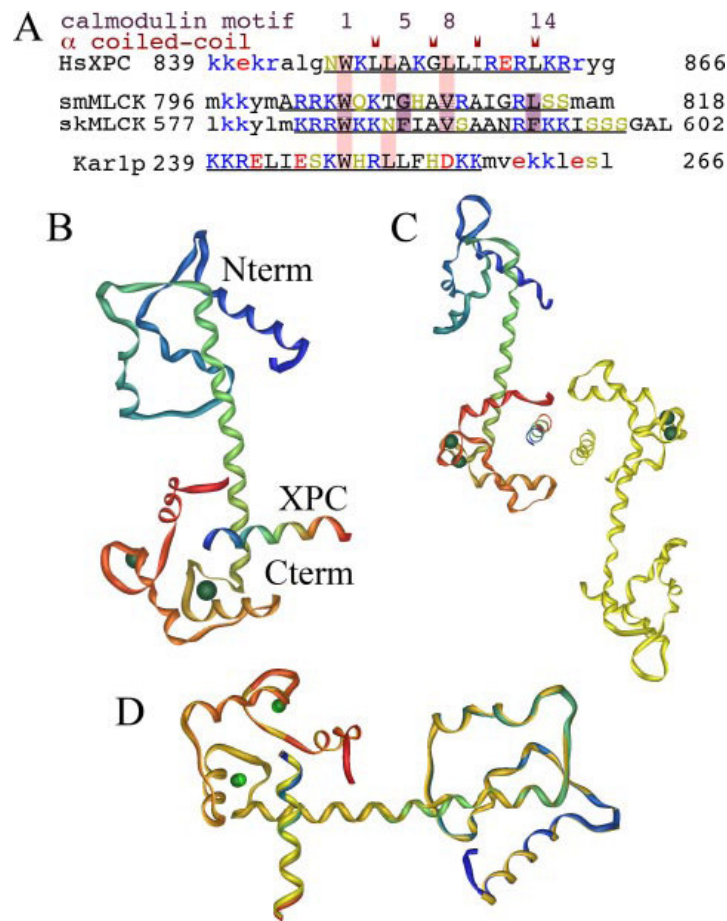


### Figure 6. Human centrin 2 and human XPC structure.

Structure of human centrin-2 bound to a human XPC-derived peptide. (A), sequence of the HsCen-2 recognition site from HsXPC structurally aligned with sequences of skeletal and smooth muscle myosin light chain kinase (*skMLCK* and *smMLCK*) and Kar1p from structures with calmodulin and yeast centrin (or caltractin). The XPC peptide structure consists of residues As<sub>1847</sub>–Arg<sub>863</sub>, the HsXPC sequence *underlined*. Essential HsXPC residues interacting to form  $\alpha$ -helical coiled-coil are indicated in *red*. *Shaded pink* are important HsXPC residues interacting with HsCen-2. Positions numbered “1-5-8-14” of key interfacial residues in skeletal muscle myosin light chain kinase and smooth muscle myosin light chain kinase bound to calmodulin are shown for comparison in *purple*. *B*, *rainbow ribbon* trace of the main chains of HsCen-2 with HsXPC and two bound Ca<sup>2+</sup> metals at the C-terminal domain. An ordered helical linker separates N-terminal (*blue*) (*N-term*) and C-terminal (*red*) (*C-term*) domains. The entire XPC peptide is  $\alpha$ -helical. *C*, two complexes are found in the asymmetric unit. They interact solely through bound XPC peptides that form an  $\alpha$ -helical coiled-coil structure. *D*, the two independent complex structures are nearly equivalent in overall conformation. *Adapted from Thompson, et. al. 2006.*

***CDC31-Sfi1p complex (yeast homologs)***

The function of centrin on centrin-based fiber contraction within the centriole is not yet understood. It is thought that Sfi1p, a centrin biological target protein may also play this role [Kilmartin, et. al. 2003]. This protein is localized within the centrosome of higher eukaryotes or the Spindle Pole Body (SPB) of yeast (Figure 7). Sfi1 is a 1242 amino acid protein comprised of 23 binding sites for centrin. These binding sites are 33 amino acids long, and are not well conserved, yet a pattern of hydrophobic residues within these sites can be established as AX<sub>2</sub>LLX<sub>3</sub>F(L)X<sub>2</sub>WK(R). Kilmartin's group (2006) studied the crystal structures of *Saccharomyces cerevisiae* centrin (Cdc31p) and Sfi1p. They describe the complexes containing several Sfi1 peptides that adopt helical contributions while bound to Cdc31. The Cdc31 proteins are wrapped around each Sfi1p repeat and have a head-to-tail arrangement with contacts amongst the neighboring Cdc31 bound proteins. The Cdc31 N-terminal domains bind to the N-terminal half of the Sfi1p repeat containing the conserved alanine residue [Li, et. al. 2006].

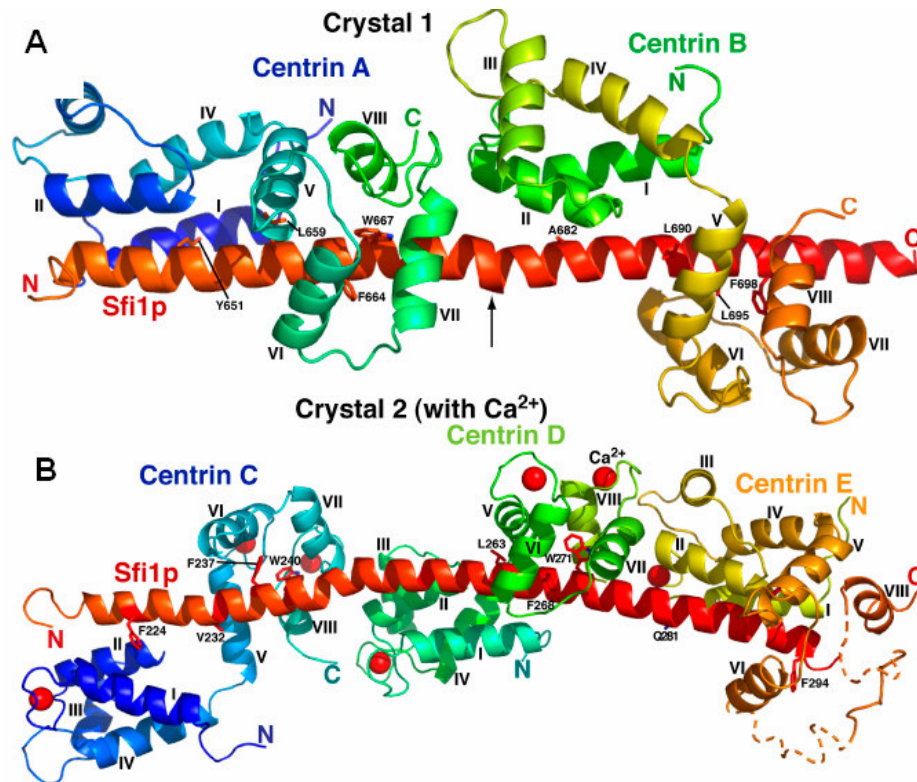


**Figure 7. Structure of the Cdc31-Sfi1p complex.**

(A) Crystal 1 Ribbon diagram of centrin-Sfi1p complex containing two Sfi1 repeats and two centrin at low Ca<sup>2+</sup> concentration. The arrow indicates a bugle and bend in the  $\alpha$ -helix. Centrin helices are marked. (B) Crystal 2. centrin-Sfi1p complex containing three Sfi1 repeats (N<sub>218</sub>-H<sub>306</sub>) and three centrins with Ca<sup>2+</sup> bound. Ca<sup>2+</sup> ions are indicated by red spheres. The end of the third Sfi1 repeat and parts of the C-terminal domain of centrin E were indistinct (dotted lines). Adapted from Kilmartin, et. al. 2006.

### ***Nuclear Magnetic Resonance (NMR)***

Nuclear Magnetic Resonance (NMR) spectroscopy is also a high resolution technique that provides macromolecular solution structures at atomic resolution. In addition, this technique provides the motion of domains of a protein as well as the exchange kinetics. From the data obtained, the three-dimensional structure can be calculated. NMR spectroscopy is limited to small (<40 kDa), stable, soluble proteins that do not aggregate at the high concentrations required for data collection.

### ***Ccen C-terminal domain and a fragment of Kar1p***

NMR spectroscopy has been used by Chazin's group to study *Chlamydomonas reinhardtii* centrin (Ccen) and how its C-terminal domain (Ccen-C) interacts with a peptide fragment of Kar1p-(239-257) [Hu, et. al. 2004 and Meyn, et. al. 2006]. Kar1p is one of the few known targets identified for centrin and is an essential component of the spindle pole body in yeast. They characterized the affinities of Ccen-C for calcium and for a peptide fragment of Kar1p and they observed the direct coupling of the calcium binding-induced shift in the equilibrium between the closed and the open conformations to the binding of the Kar1p peptide. They describe that centrin is constitutively bound to Kar1p through its C-terminal domain and its N-terminal domain is the calcium sensor [Hu, et. al. 2004].

Changes in the structure of C-terminal Ccen after phosphorylation at Ser<sub>167</sub> using NMR spectroscopy were determined by Chaizin's group in collaboration with our group. The

effect of the phosphorylation on target binding in the Ccen-C-Kar1p complex was also determined. The comparisons of NMR chemical shift differences induced by phosphorylation have a greater effect from phosphorylation in the context of the kar1p complex than the free protein. They also observed that Ccen-C in complex with Kar1p can not be phosphorylated [Meyn, et. al. 2006].

### ***Ccen N-terminal domain and a fragment of Sfi1***

Sheehan, et. al. (2006) determined the three-dimensional structure of the N-terminal domain of Ccen in the presence of calcium by solution NMR spectroscopy. The domain occupies an open conformation similar to EF-hand calcium domains. The N-terminal domain and C-terminal domain have domain specificity of interactions with its cellular targets due to structural and biochemical differences. They characterized the interaction of Ccen-N with seventh centrin binding repeat of Sfi1 by titration using NMR spectroscopy. Sfi1 binds to a discrete site on the protein, which support the proposal that the N-terminal domain serves as a calcium sensor in centrin [Sheehan, et. al. 2006].

### ***Hcen2 - hSfi1p complexes***

Martinez-Sanz, et.al. (2006) studied the binding of Hcen2 to HSfi1 using NMR spectroscopy (Figure 8). These studies explored peptides comprised of binding sites R<sub>1</sub> (111-130), R<sub>12</sub> (475-494), and R<sub>17</sub> (641-660), corresponding to HSfi1p centrin binding sites 1,

12 and 17, are bound independently to one centrin molecule. Hcen2 carboxy-terminal domain interacts hydrophobically with Trp<sub>11</sub> within HSfi1p repeat [Martinez-Sanz, et. al. 2006], while HSfi1p comprised of R<sub>12</sub> (475-494) binding site did not bind centrin. It is thought that the proline residue located in a central position affects the binding of centrin.

It is important to note that the NMR studies carried-out for centrin and the centrin complexes have been for the terminal domain peptides due to the intrinsic flexibility of the protein.

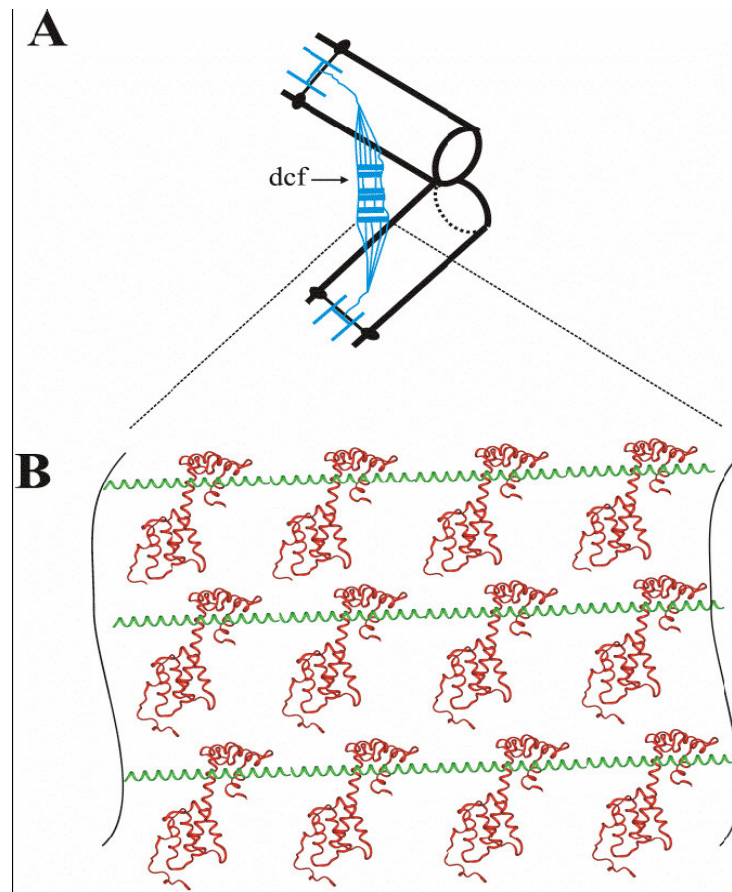


**Figure 8. Working model of the protein multimeric assembly including centrin and Sfi1 in the contractile fibres of the basal bodies.**

(A) Simplified scheme of the basal body ultrastructure with the distal connecting fibres in blue. (B) Model of contractile fibres with long Sfi1 helices (green) and centrin molecules (red) bound through their C-terminal domain. The longitudinal contraction of the assembly may be induced by the  $\text{Ca}^{+2}$ -dependent homo-molecular centrin interactions. Adapted from Martinez-Sanz, et. al. 2006.

### ***Fourier-Transform Infrared (FT-IR) Spectroscopy***

Other techniques are used to study proteins; among these is Fourier-Transform infrared (FT-IR) spectroscopy. Pastrana-Rios, group has used FT-IR spectroscopy and two-dimensional correlation analysis to study centrin [Ocaña, et. al. 2002; Pastrana-Rios, et. al. 2002; Ortiz, et. al. 2002; Ortiz, et. al. 2005, Sanoguet, et. al. 2006 and Sosa, et. al. 2006]. The secondary structure composition of Ccen has been determined as 60%  $\alpha$ -helix, 12%  $\beta$ -sheets, 14.7%  $\beta$ -turn, and 13% random coil, in presence of cations. They also observed the monodentate coordination of aspartate to cation and demonstrated a reversible conformational pre-transition for Ccen (37°C in apo- and 45°C in holo- forms), thus, establishing that centrin in the presence of cations is more stable than centrin in its apo state [Ocaña, et. al. 2002 and Pastrana-Rios, et. al. 2002]. They also observed an exclusive  $3_{10}$ -helix (1650  $\text{cm}^{-1}$ ) contribution in the C-terminal domain when they compared the Hydrogen/Deuterium exchange dynamics with N-terminal domain. A minor exposure to its aqueous environment due to self-association was also observed in the C-terminal domain [Ortiz, et. al. 2002 and Ortiz, et. al. 2005]. When Ccen is phosphorylated at Ser<sub>167</sub> the aspartate and glutamate side chains located in the calcium binding loop IV are affected by phosphorylation. This loop and the C-terminal end  $\alpha$ -helical motif (1650  $\text{cm}^{-1}$ ) are less stable in the phosphorylated form than the unphosphorylated form [Sanoguet, et. al. 2006].

The interaction of Ccen full length with a bee venom peptide known as melittin was also studied using FT-IR spectroscopy. This interaction was driven by the effects on the  $\alpha$ -

helical motifs of centrin by melittin to a greater extent than its interaction with calcium [Sosa, et. al. 2006].

### Infrared spectroscopy

IR spectroscopy is based on the IR light absorption by the molecules. The absorption occurs when the light frequency match with the vibration frequency of molecules and it is usually plotted against the wavenumber  $\tilde{\nu} = 1/\lambda$  (in units of  $\text{cm}^{-1}$ ) which is inverse of the wavelength  $\lambda$ . The vibration frequency and the absorption probability depend on the strength and polarity of the vibrating bonds. The fundamental principles that govern the relationship between the vibrational spectrum of a molecule and its structure and environment are illustrated by the simple diatomic oscillator.

$$\nu = \frac{\sqrt{(k / \mu)}}{2\pi} \quad (1)$$

where  $\nu$ , is the frequency of a diatomic oscillator,  $k$  is the constant force between the two atoms, and  $\mu$  is the reduced mass

$$\mu = \frac{m_1 m_2}{m_1 + m_2} \quad (2)$$

The frequency is also influenced by the mass of the vibrating atoms. The larger the mass, the faster the frequency of vibration. Thus, vibrational spectroscopy is sensitive to isotope effects [Barth, et. al. 2002 and Arrondo, et. al. 1999].

IR spectroscopy is useful for the study of proteins offering a wealth of information about protein conformation, environment of side chains, and protein-protein interactions. Infrared spectroscopy is routinely used to evaluate changes in proteins induced by temperature, pH, ligand binding, etc. and it is not limited by size of protein, amount of proteins (typically 1mg depending of protein), physical state, or environment of the protein sample.

Proteins can be studied using IR spectroscopy because they are comprised of functional (amide) groups that posses highly localized vibrations that complicate the band assignment and the observed changes thereof.

N-methylacetamide, the simplest molecule containing an amide group, has been studied to characterize the vibrational modes of this group (Figure 9) [Krimm, et. al. 1986]. Nine IR bands, which are termed “amide bands”, have been established (Table 1). The amide bands are due to different amide group vibrational modes within the peptide bond.

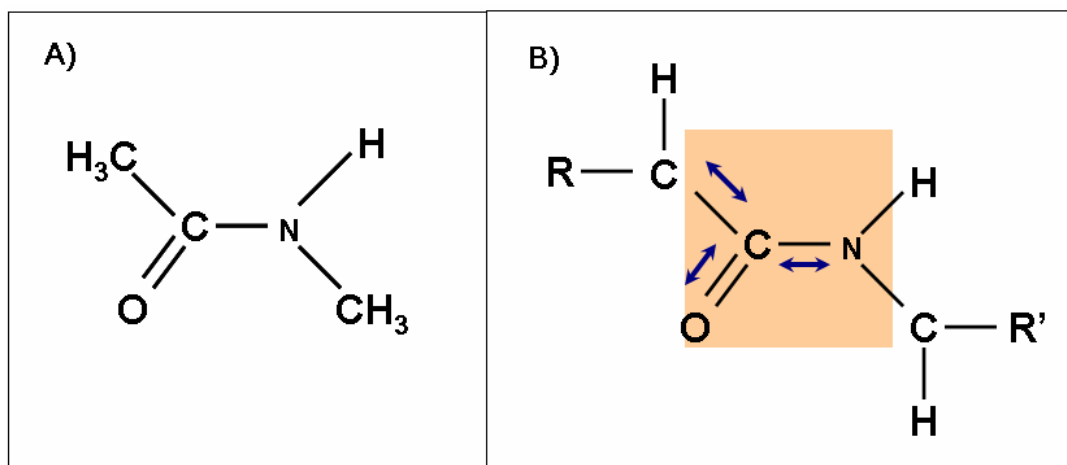


**Figure 9. *N*-methylacetamide and peptide bond similarity.**

A) Structure of *N*-methylacetamide (NMA). Observe the similarity with a peptide bond. B) Schematic representation of a peptide bond which is the result of the polymerization of amino acids. The arrows denote the vibrations contributing to the amide I band.

Table 1. Characteristic IR amide bands of the peptide linkage, based in the spectrum of *N*-methylacetamide. (Heinz, F. and Mäntel, W. 2002)

Nomenclature (Amide)	Approximate wavenumber ( $\text{cm}^{-1}$ )	Vibrational modes
A	~ 3300	NH stretching in resonance with 1 <sup>st</sup> amide II
B	~ 3100	overtone
I	1610 - 1695	CO stretching
II	1480 - 1575	NH bending and CN stretching
III	1220 - 1320	CN stretching and NH bending
IV	625 - 765	OCN bending, mixed with other modes
V	640 - 800	Out of plane NH bending
VI	335 - 605	Out of plane CO bending
VII	~ 200	Skeletal torsion

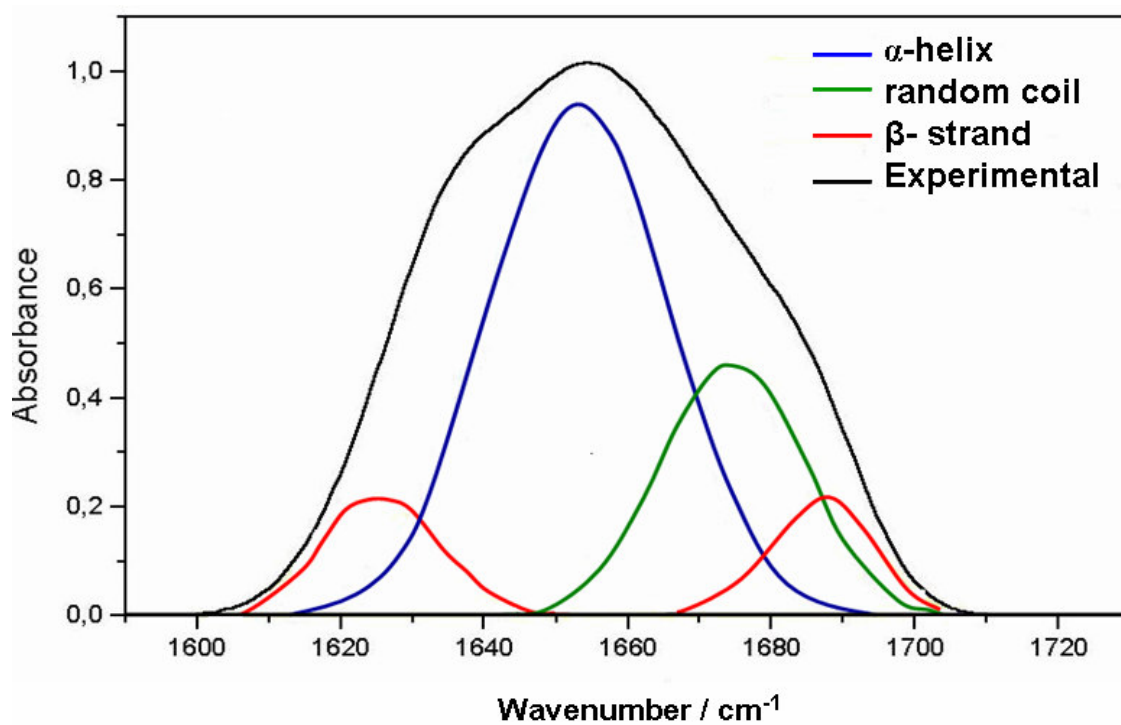


**Figure 10. Different components of the amide I band.**

Overlay of experimental and simulated spectrum with contributing subbands.

The two most studied bands are amide I and amide II. These have the highest molar extinction coefficient for proteins within the IR spectrum. The amide I band is a complex band with several vibrational contributions that correspond to various structural elements in a protein (Figure 10). This band is sensitive to secondary structure composition and therefore, most commonly used for secondary-structure analysis [Barth, et. al. 2002, Heinz, et. al. 2002].

IR studies of proteins in water are complicated by the fact that the H-O-H bending vibration of H<sub>2</sub>O absorbs strongly at 1645 cm<sup>-1</sup>, thus overlapping the amide I and II spectral region. To resolve this problem, a short pathlength (3 – 8 μm) is used for transmission measurements in the amide I region and limit the overlap of H<sub>2</sub>O I absorption in this spectral region. A second alternative is the use of deuterium oxide (D<sub>2</sub>O) protein solutions, where, the D-O-D bending vibration occurs at lower wavenumbers (1215 cm<sup>-1</sup>) thus, eliminating the overlap with the amide I region (1600 – 1700 cm<sup>-1</sup>). Typically, longer pathlengths (40 – 80 μm) are used. The H/D exchange causes a shift of the amide I band to lower wavenumbers (1650 – 1640 cm<sup>-1</sup>) due to the underlying 20% N-H bending contribution within the amide I band (1650 cm<sup>-1</sup>) and consequently termed amide I' band (1640 cm<sup>-1</sup>). More importantly, the use of D<sub>2</sub>O as an aqueous solvent allows the spectroscopist to study the side chain modes found within the amide II' band (1600-1500 cm<sup>-1</sup>) after complete H/D exchange of the protein sample. Therefore, the amide II band (1550 cm<sup>-1</sup>), comprised mainly of N-H deformation and C-N modes shifts to 1450 cm<sup>-1</sup> and termed amide II' band, due to N-D deformation bending mode. [Chirgadze, et. al. 1975, Kabsch, et. al. 1983,

Arrondo, et. al. 1993, 1999, Heinz, et.al. 2002, Goormaghtigh, et. al. 1999, Pastrana-Rios, et. al. 2001, 2002, 2006, Sanoguet, 2006].

***Hydrogen / deuterium exchange of the protein sample.***

***A) Amide I' band***

The amide I and amide I' are the best characterized bands that provide information about secondary structure of proteins because of their sensitivity to hydrogen-bonding pattern, dipole-dipole interaction and the geometry of the polypeptide backbone. The shift of the amide I band is relatively small from 5 cm<sup>-1</sup> to 10 cm<sup>-1</sup>, and this band is then called amide I'. The amide I/I' band of proteins consist of a series of overlapping components bands that represent different structural elements, such as,  $\alpha$ -helix,  $\beta$ -sheets,  $\beta$ -turns and disordered structures, which occur as result of different conformation states present in the protein of interest (Table 2).

***B) Amide II' band***

In proteins, side chain modes are generally of low intensity. The contribution of amino acids side chains depend on their protonation state; however, their absorption provides valuable information about protein molecular reaction mechanism, environment

and coordination state to divalent cations [Barth, et. al. 2002, Pastrana-Rios, et. al. 2002, Ortiz, et. al. 2005, Nabet, et. al. 1997, Raussens, et. al. 2004, Vigano, et. al. 2004]. The associated side chains bands are listed in the Table 3.

Table 2. **Assignment of amide I/I' band positions to secondary structure.** (Barth, et.al 2002, Arrondo, et. al. 1993, Heinz, et. al. 2002, Lee, et. al. 1986)

Secondary structure	Band position in H <sub>2</sub> O (cm <sup>-1</sup> )		Band position in D <sub>2</sub> O (cm <sup>-1</sup> )	
	Average	Extremes	Average	Extremes
α-helix	1654	1648 – 1657	1652	1642 -1660
β-sheets	1633	1623 – 1641	1630	1615 - 1635
β-sheets	1684	1674 – 1695	1679	1672 - 1694
β-turns	1672	1662 – 1686	1671	1653 -1691
Disordered	1654	1642 – 1657	1645	1639 - 1654

Table 3. Position of amino acid side chains IR bands present in the Amide I/I' region. (Chrigadze, et. al. 1975, Barth, et. al. 2002)

Assignments	Band Position in H <sub>2</sub> O (cm <sup>-1</sup> )	Band Position in D <sub>2</sub> O (cm <sup>-1</sup> )
Asn, $\nu(\text{C=O})$	1677 – 1678	1648
Arg, $\nu_{\text{as}}(\text{CN}_3\text{H}_5^+)$	1652 – 1695	1605 - 1608
Gln, $\nu(\text{C=O})$	1668 – 1687	1635 - 1654
Arg, $\nu_{\text{s}}(\text{CN}_3\text{H}_5^+)$	1614 – 1663	1581 – 1586
HisH <sub>2</sub> <sup>+</sup> , $\nu(\text{C=C})$	1631	1600, 1623
Lys, $\delta_{\text{as}}(\text{NH}_3^+)$	1626 – 1629	1201
Tyr-OH, $\nu(\text{CC}) \delta(\text{CH})$	1614 – 1621	1612 – 1618
Asn, $\delta(\text{NH}_2)$	1612 – 1622	----
Trp, $\nu(\text{CC}), \nu(\text{C=C})$	1622	1618
Tyr-O <sup>-</sup> , $\nu(\text{CC})$	1599 – 1602	1603
Tyr-OH, $\nu(\text{CC})$	1594 – 1602	1590 – 1591
Gln, $\delta(\text{NH}_2)$	1586 – 1610	1163
HisH, $\nu(\text{C=C})$	1575, 1594	1569, 1575
Asp, $\nu_{\text{as}}(\text{COO}^-)$	1574 – 1579	1584
Glu, $\nu_{\text{as}}(\text{COO}^-)$	1556 – 1560	1567

$\nu$ , stretching vibration;  $\nu_{\text{s}}$ , symmetric stretching vibration;  $\nu_{\text{as}}$ , antisymmetric stretching vibration;  $\delta$ , in-plane bending vibration;  $\delta_{\text{a}}$ , asymmetric in-plane bending vibration.

---- Not observed

## Two-Dimensional Correlation Spectroscopy

Two-Dimensional Correlation spectroscopy (2D-COS) has been routinely used in our laboratory for spectroscopic data analysis. This 2D-COS analysis method was developed by Dr. Isao Noda and is based on the detection of dynamic variations of spectroscopic signals induced by an external perturbation where the IR radiation is used as a probe [Noda, et. al. 2000]. The external perturbation can be any perturbation that modifies the spectrum, such as, temperature, pressure, chemical, acoustics, etc. The correlation analysis of spectral fluctuations leads to 2D plots that increase the spectral resolution by spreading peaks along a second dimension and that reveal the order of the actual sequence of events induced by the perturbation, as summarized in Figure 11.

Two types of spectral representation are obtained, synchronous (represented by  $\Phi$ ) that is comprised of in phase intensity changes (Figure 10) and asynchronous (represented by  $\Psi$ ) that is out of phase intensity changes (Figure 11). These correlational plots are generated as a function of two axes ( $\nu_1, \nu_2$ ) where,  $\nu_1$  represents the initial spectrum before the system perturbation and  $\nu_2$  represents the spectrum at the end of perturbation [Heinz, et. al. 2002].

Two-dimensional correlation is generated by a formal mathematical procedure where a reference spectrum  $\bar{y}(\nu)$  (3) is used to generate a dynamic spectrum  $\tilde{y}(\nu, t)$  (4) which is due to a perturbation-induced change of the spectral intensity  $y(\nu, t)$  an interval of some external variable  $t$  between  $T_{\min}$  and  $T_{\max}$ . In this dynamic spectrum  $t$  is the chronological variable, and  $\nu$  can be any appropriate index quantity.

*Reference spectrum*

$$\tilde{y}(v) = \frac{1}{T_{\max} - T_{\min}} \int_{T_{\min}}^{T_{\max}} y(v, t) dt \quad (3)$$

*Dynamic spectrum*

$$\tilde{y}(v, t) = \begin{cases} y(v, t) - \bar{y}(v) & \text{For } T_{\min} \leq t \leq T_{\max} \\ 0 & \text{otherwise} \end{cases} \quad (4)$$

Once the dynamic spectrum is generated the correlation is made by comparative mathematical analysis from similarity or dissimilarity of the spectral intensity variations measure at two different wavenumbers during fixed interval (5). Mathematically, this expression is simplified by two orthogonal coordinates complex number which arise the two-dimensional plots known as: synchronous ( $\Phi$ ) and asynchronous ( $\Psi$ ) (6).

*Correlation function*

$$X(v_1, v_2) = \langle \tilde{y}(v_1, t) \bullet \tilde{y}(v_2, t') \rangle \quad (5)$$

*Generalized two-dimensional correlation function*

$$X(v_1, v_2) = \Phi(v_1, v_2) + i\Psi(v_1, v_2) = \frac{1}{\pi(T_{\max} - T_{\min})} \int_0^{\infty} \tilde{Y}_1(\omega) \bullet \tilde{Y}_2(\omega) d\omega \quad (6)$$

A Fourier transform of the spectral intensity variations ( $\tilde{Y}_2(\omega)$ ) observed at a wavenumber respect to external perturbation is an implicit function in the generalized two-dimensional correlation equation. In order to achieve an adequate numerical estimation of two-dimensional correlation intensity, a matrix approximation through vectors is used in this algorithm (7). Therefore, a computationally efficient equations set is generated to calculation of synchronous (8) and asynchronous plot (9).

*Dynamic spectrum matrix representation*

$$\tilde{Y}(v) = \begin{bmatrix} \tilde{y}(v, t_1) \\ \tilde{y}(v, t_2) \\ \dots \\ y(v, t_m) \end{bmatrix} \quad (7)$$

*Equations of vector notation for synchronous and asynchronous plot.*

$$\Phi(v_1, v_2) = \frac{1}{m-1} \tilde{Y}(v_1)^T \tilde{Y}(v_2) \quad (8)$$

$$\Psi(v_1, v_2) = \frac{1}{m-1} \tilde{Y}(v_1)^T N \tilde{Y}(v_2) \quad (9)$$

*Hilbert-Noda transformation matrix for synchronous plot acquisition*

$$N_{jk} = \begin{cases} 0 & \text{If } j=k \\ 1/\pi(k-j) & \text{Otherwise} \end{cases} \quad (10)$$

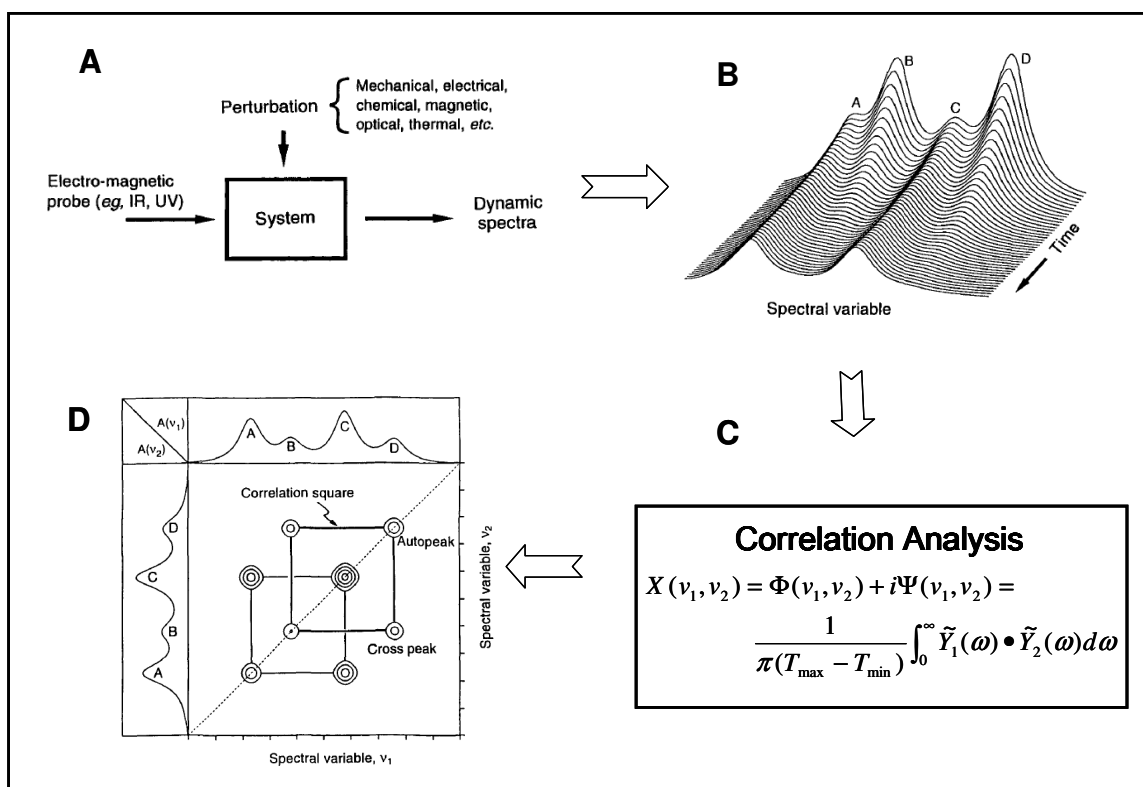


**Figure 11. General scheme for obtaining 2D correlational plots**

A) An external perturbation is needed to obtain a dynamic spectra. B) The dynamic spectra is generated in a sequential manner. C) General equation for the 2D correlation analysis. D) Synchronous plot generated from the real component of the equation. (Noda, et. al. 2000).

The synchronous ( $\Phi$ ) plot is characterized by their symmetry and autopeaks located on the diagonal. The magnitude of the autopeak intensity, which is always positive, represents the overall extent of spectral intensity variation observed during the perturbation. On both sides of diagonal are the cross peaks that appear when two bands are correlated. These peaks can be either positive or negative. Where the positive cross peaks represents intensity changes, peak position and bandwidth changes that occur simultaneously and in the same direction as the autopeaks involved. Where the negative cross peaks constitutes changes in peak intensity, peak position and bandwidth changes that occur due to a decrease in intensity (Figure 12).

The asynchronous plot ( $\Psi$ ) (Figure 11) is antisymmetric and has no autopeaks, consisting exclusively of cross peaks located in off-diagonal positions within the plot. These cross peaks represent out of phase changes between two peaks. Like synchronous plot, in asynchronous plot the cross peaks can be positive or negative. A positive cross peak if the intensity change at  $\nu_1$  (x axes) occurs before  $\nu_2$  (y axes). A negative cross peak, on the other hand, if the changes at  $\nu_1$  (x axes) occur after  $\nu_2$  (y axes). This rule, however, is reversed if  $\Phi(\nu_1, \nu_2) < 0$ , that is when the position of asymmetric peak is transferred to synchronous plot is located in the negative area (Figure 13) [Heinz, et. al. 2002, Noda, et. al. 2000].

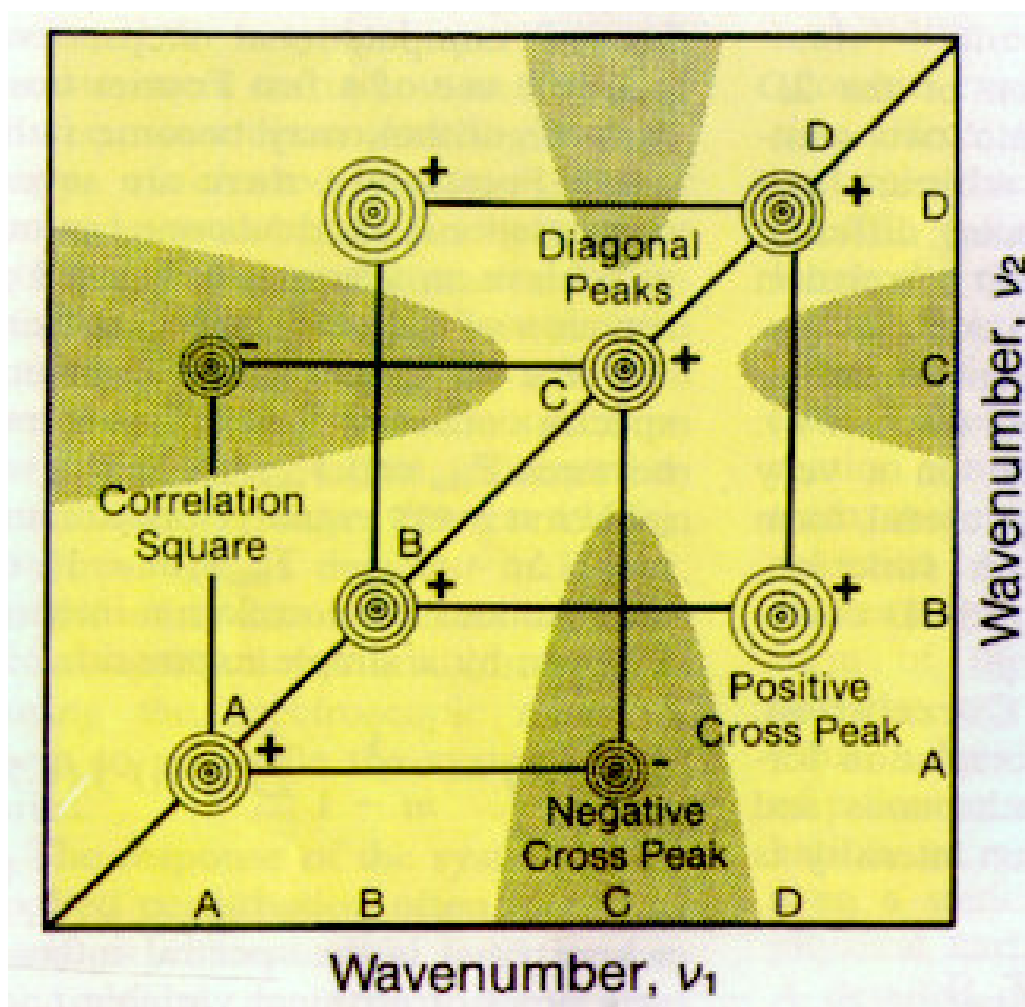


Figure 12. Schematic synchronous contour plot of a hypothetical two-dimensional correlation analysis. (Noda, et.al. 2000)

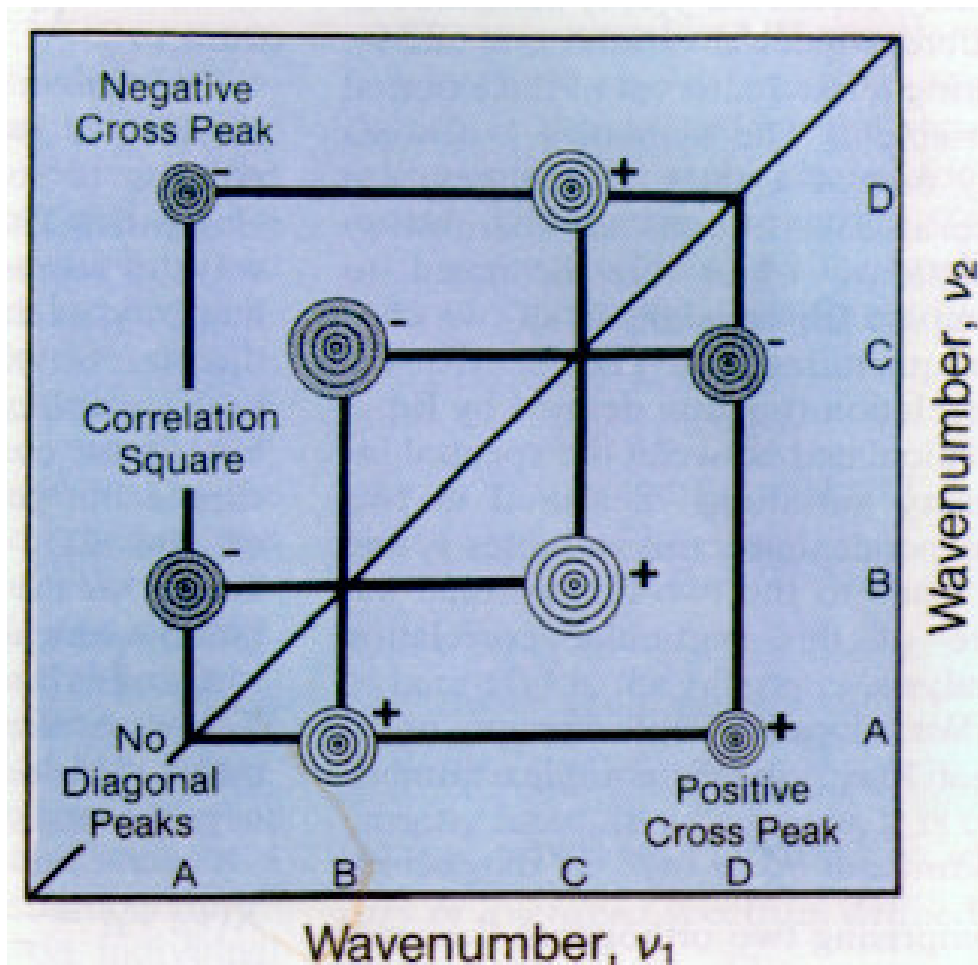


Figure 13. Schematic of an asynchronous contour plot using a hypothetical two-dimensional correlation analysis. (Noda, et.al. 2000)

## CHAPTER III

### MATERIALS AND METHODS

#### Bacterial expression of Human centrin 1 and 2

Overnight cultures were prepared as follows: 200  $\mu$ L of a bacterial stock of newly transformed competent cells *E.coli* BL21-RIL (DE3) with pT7-7-Hcen1 or pT7-7-Hcen2 were used to inoculate 250 mL of 2xYT media (BIO 101, Inc., Carlsbad, CA) containing 50  $\mu$ g/mL of ampicilin and incubated in an orbital shaker at 37°C at 250 rpm for a period of twelve hours.

Using a bioreactor BIOFLO 3000 (New Brunswick Scientific, Edison, NJ), the overnight culture was inoculated in 4.75 L of sterile 2xYT media which contain 50  $\mu$ g/mL of ampicilin. The bacterial growth was performed at 37°C, 350 rpm of agitation, water flow setting at maximum pressure of 20 psi, air and oxygen gas were set at a maximum pressure of 10 psi, the dissolved oxygen (D<sub>2</sub>O) was set to 100%, at pH 7.00, when necessary the pH was adjusted with 30% NH<sub>4</sub>OH and 2.5M KH<sub>2</sub>PO<sub>4</sub>. The cell growth was monitored *via* optical density (OD) at 550 nm, when the cells reached *log* phase they were induced with 0.5 mM isopropyl- $\beta$ -D-thiogalactopyranoside (IPTG). Typically, three hours later the cells were harvested by centrifugation for 20 minutes at 3,500 rpm (2465x g) at 4°C using a J-10 rotor and a Beckman J2-MC centrifuge. The pelleted cells obtained were stored at -80°C, for subsequent purification.

## Isolation and Purification of Human centrin 1 and 2

The frozen pellets of Hcen1 or Hcen2 were thawed in lysis buffer (50 mM Tris, 0.5 mM EDTA, 0.5 M NaCl, 0.04% NaN<sub>3</sub> and 0.1% IGEPAL at pH 7.4) containing a cocktail of protease inhibitors (2.0 mg/mL aprotinin, 0.5 mg/mL leupeptin, 1.0 mg/mL pepstatin A, 2  $\mu$ L pefabloc SC per milliliter of crude lysate) and sonicated with a Branson sonifier model 450 (Branson Ultrasonics Co., Danbury, CT) 3x 30 s pulses at maximum power and 1 min rest periods while on ice. The whole cell lysate was then centrifuged at 10 000 rpm (9 615x g) for 15 minutes at 4°C using a JA-14 rotor and a Beckman J2-MC centrifuge. The supernatant was recovered and buffer conditions were changed to contain 4 mM MgCl<sub>2</sub> and 2 mM CaCl<sub>2</sub> followed by an ultracentrifugation step at 31,000 rpm (70 588x g) for 30 minutes at 4°C using a TI-70 rotor and a Beckman L-80 ultracentrifuge. This second supernatant was filtered using a low protein binding PES (Polyethersulfone) membrane filter with 0.22  $\mu$ m pore size.

The purification protocol has been summarized in Pastrana-Rios, et. al. 2002. Briefly, as with *Chlamydomonas* centrin, an affinity chromatography was used to further purify the desired human isoforms. The filtrate obtained was applied to Phenyl Sepharose column CL-4B (Sigma, St Louis, MO). The column was equilibrated with a buffer solution containing 50 mM Tris, 0.5 M NaCl, 4.0 mM MgCl<sub>2</sub>, 2.0 mM CaCl<sub>2</sub>, 0.1% IGEPAL and 0.04% NaN<sub>3</sub> at pH 7.4. Hcen1 and Hcen2 were eluted using a buffer solution containing 50 mM Tris, 0.5 mM EDTA, 0.5 M NaCl, 4.0 mM MgCl<sub>2</sub>, 5 mM EGTA and 0.04% NaN<sub>3</sub> at pH 7.4. To identify the

fractions containing centrin, a microfluidic Lab-chip electrophoresis from Agilent Technologies was used.

The fractions containing centrin were pooled, concentrated, re-equilibrated in a buffer containing 20 mM Hepes, 1 mM CaCl<sub>2</sub> and 1 mM DTT at pH 7.4 and subjected to a second chromatographic purification process using a strong anion-exchange (High Q) column (Bio-Rad, Hercules, CA). Centrin elution was obtained using a 0 – 0.75 N NaCl gradient. The column was then washed with 1 N NaCl. The collected fractions were analyzed by Lab-chip electrophoresis from Agilent Technologies.

Fractions containing centrin were pooled and subjected to UV analysis and Matrix Assisted Laser Desorption/Ionization Time-of-Flight (MALDI-TOF) mass spectrometry to verify its purity and integrity or oligomeric state. The MALDI-TOF mass spectrometry was performed at the MS facility at Vanderbilt University.

Purified centrin was dialyzed against a buffer solution containing 50 mM Hepes, 150 mM NaCl, 4 mM CaCl<sub>2</sub> and 4 mM MgCl<sub>2</sub> at pH 7.4 and concentrated using Millipore centrifugal device with a 5,000 MW cut off. The protein concentration was determined by UV absorbance at 274 nm using a JASCO UV/Vis spectrophotometer. The calculated molar extinction coefficient used was 1530 M<sup>-1</sup> cm<sup>-1</sup> in presence of cations. The centrin sample was lyophilized and stored at -20°C.

## FT-IR Spectroscopy

The protein sample was dialyzed under desired conditions and then lyophilized repeatedly while redissolving the sample in D<sub>2</sub>O (99% atom D). The spectra were collected following complete Hydrogen→Deuterium (H→D) exchange of the centrin sample. Approximately 1.5 mg of Hcen1 or Hcen2 in 50 mM Hepes, 150 mM NaCl, 4 mM MgCl<sub>2</sub> and 4 mM CaCl<sub>2</sub> at pD 6.6 was deposited on a 49 x 4 mm custom milled CaF<sub>2</sub> windows from Spectral System, Hopewell Junction, NJ, with a fixed path length of 40 μm. The reference was prepared similarly and set in a custom dual chamber cell holder. The temperature within the cell was controlled using a Neslab RTE-740 Refrigerated circulating bath from Thermo Electron Corp., (Madison, Wisconsin), and monitored with a thermocouple sensor from Physitemp Model Bat-12 (Clifton, NJ), positioned in a close contact with the sample. The temperature accuracy was estimated to be within 1°C.

The sample and reference spectra were obtained using a Mattson Infinity Series FT-IR spectrophotometer equipped with a mercury cadmium telluride (MCT) detector, a sample shuttle, and a PC interface. Spectral acquisition was done at sequential increments of temperature from 0.5 °C to 88 °C. Routinely, 10 min was allowed for thermal equilibrium to be reached prior to spectral acquisition. Typically, 512 scans were coadded, apodized with a triangular function, and Fourier transformed to provide a resolution of 4 cm<sup>-1</sup> with data encoded every 2 cm<sup>-1</sup>.

## **Data Analysis**

For spectral baseline correction and 2D-COS analysis, a computer program known as Kinetics for MATLAB (The MathWorks, Natick, MA) generously provided by Dr. Erik Goormaghtigh from the Free University of Brussels, Belgium was used.

## CHAPTER IV

### RESULTS AND DISCUSSIONS

#### Bacterial expression of Human centrin 1 and 2

The high level expression of Hcen1 and Hcen2 was carried out using a bioreactor BIOFLO 3000 (New Brunswick Scientific, Edison, NJ) and a high yield cell culture was achieved obtaining 41.46 g of pellet for Hcen1 and 17.10 g of pellet for Hcen2. Transformed competent cells *E.coli* BL21-RIL (DE3) with pT7-7-Hcen1 for Hcen1 and *E.coli* BL21-RIL (DE3) with pT7-7-Hcen2 for Hcen2 were grown in 2xYT media (BIO 101, Inc., Carlsbad, CA) containing 50 µg/mL of ampicilin. The cell growth was monitored every 30 min by optical density (OD) at 550 nm (Figure 14 and 16).

At the beginning of the log phase the cells were induced with 0.5 mM isopropyl-β-D-thiogalactopyranoside (IPTG). The induction of Hcen1 expression was performed 2.5 hr after inoculation (Figure 14) and for Hcen2 1.5 hr after inoculation the bacterial cell were induced (Figure 16). Aliquots were taken every 30 min during the time course of high level expression of the desire human recombinant protein. These aliquots were later lysed and analyzed by 15% SDS-PAGE. The increment in the protein production was observed after induction for Hcen1 (Figure 15) and Hcen2 (Figure 17). Once the cells reached the stationary phase the cells were harvested for Hcen1 7.5 hrs (41.5 g) after being induced

while for Hcen2 it was THREE hrs (17.1 g) after induction. This accounted for the different cells in protein yield.

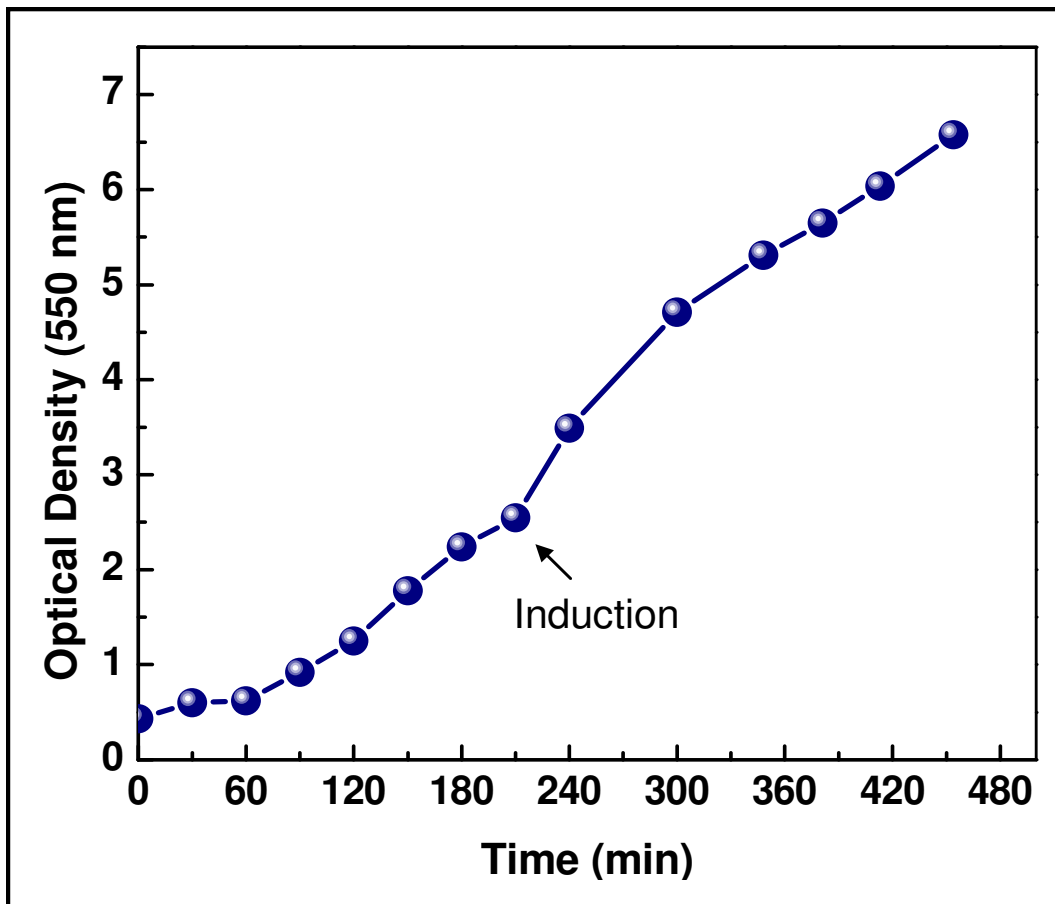


**Figure 14. Hcen 1 growth curve plot.**

Growth curve plot of transformed cells *E. coli* BL21-RIL (DE3) with pT7-7-Hcen1 obtained by measuring optical density at 550 nm. The arrow shows the induction point 4 hrs after inoculation.

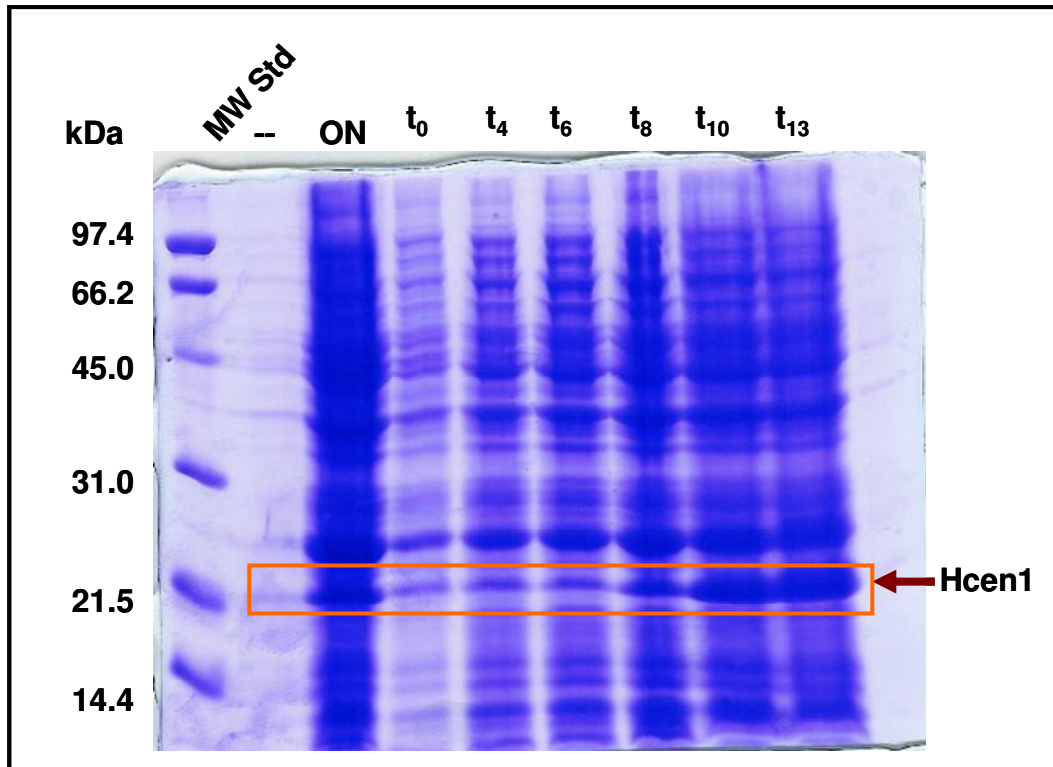


**Figure 15. SDS-PAGE Hcen 1 high level expression.**

5 -15% SDS-PAGE of the Hcen1 high level expression time course. Where t<sub>0</sub>, t<sub>4</sub>, t<sub>6</sub>, t<sub>8</sub>, t<sub>10</sub>, and t<sub>13</sub> corresponding to times 0, 120, 180, 240, 348 and 454 min respectively. Molecular weight standard (MW Std), over night culture (ON), cell lysates of progressive expression prior induction (t<sub>0</sub>, t<sub>4</sub> and t<sub>6</sub>), and cell lysates of progressive expression after induction (t<sub>8</sub>, t<sub>10</sub> and t<sub>13</sub>). Parallel to 21.5 band of the marker can be observed the over-expression of Hcen1.

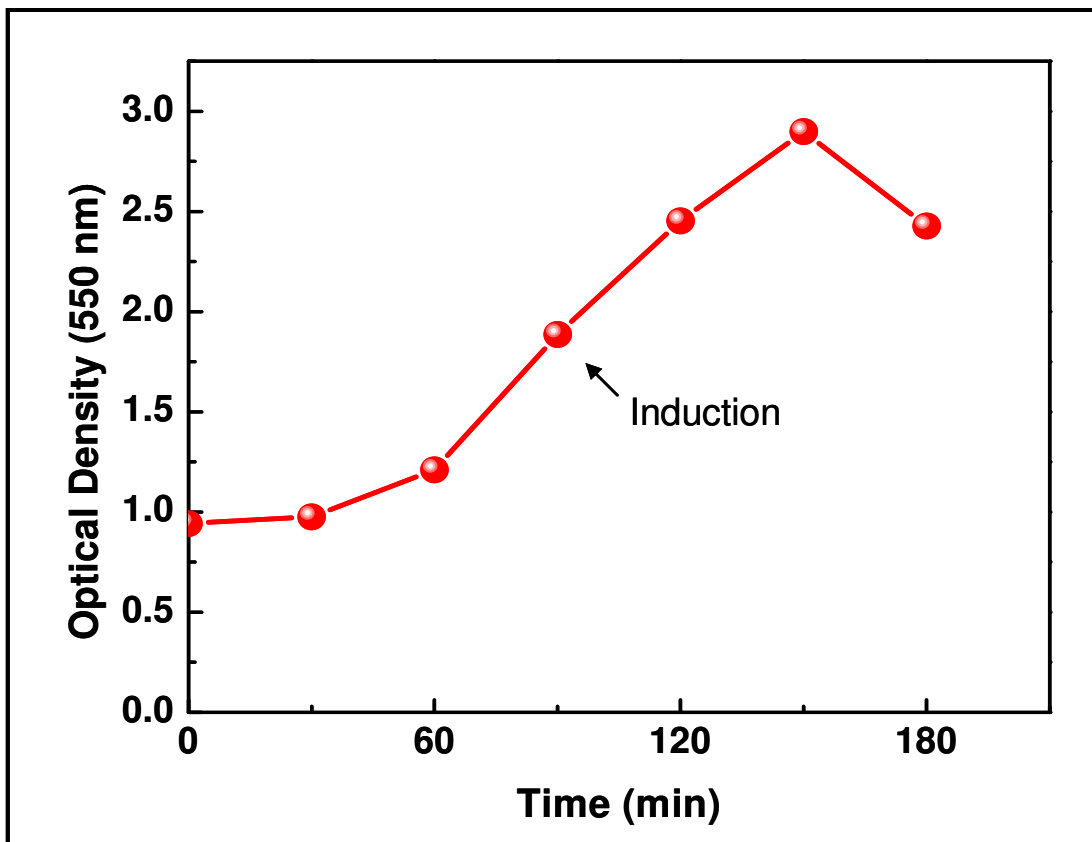


**Figure 16. Hcen 2 growth curve plot.**

Growth curve plot of transformed cells *E.coli* BL21-RIL (DE3) with pT7-7-Hcen2 obtained by measuring optical density at 550 nm. The arrow shows the induction point 1.5 hrs after inoculation.

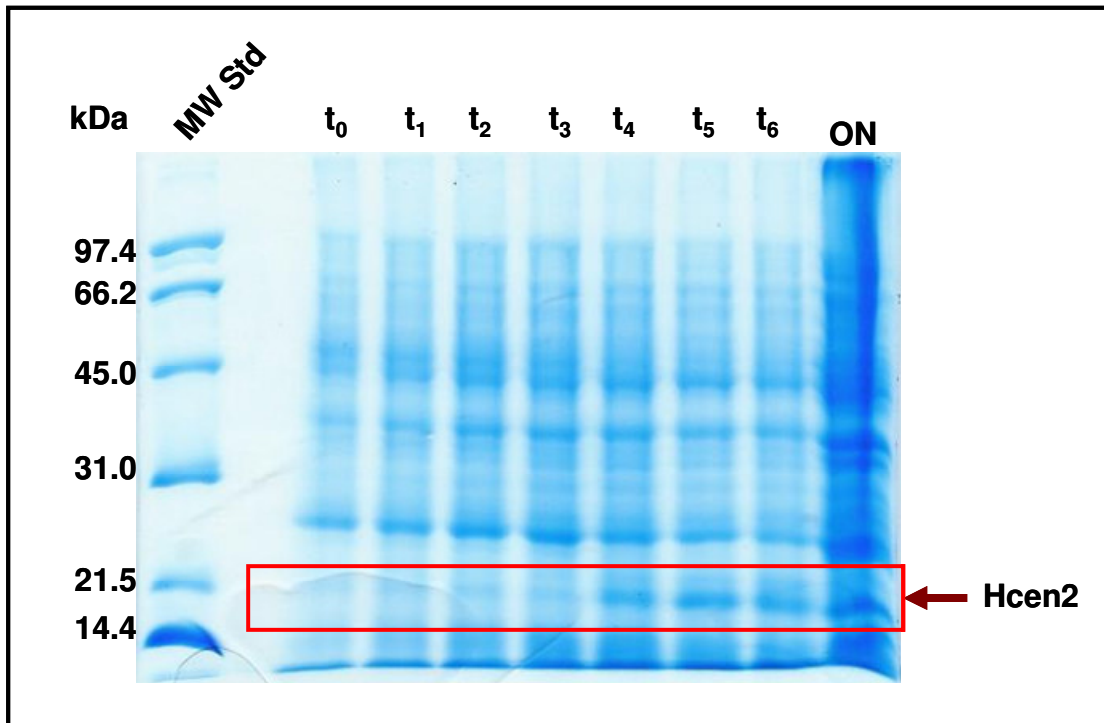


**Figure 17. SDS-PAGE Hcen 2 high level expression.**

5 - 15% SDS-PAGE of the Hcen2 high level expression time course. Where t<sub>0</sub>, t<sub>1</sub>, t<sub>2</sub>, t<sub>3</sub>, t<sub>4</sub>, t<sub>5</sub> and t<sub>6</sub> corresponding to times 0, 30, 60, 90, 120, 150 and 180 min respectively. Molecular weight standard (MW Std), cell lysates of progressive expression prior induction (t<sub>0</sub>, t<sub>1</sub> and t<sub>2</sub>), cell lysates of progressive expression at time induction (T<sub>3</sub>), cell lysates of progressive expression after induction (t<sub>4</sub>, t<sub>5</sub> and t<sub>6</sub>), and over night (ON) culture. Parallel to 21.5 kDa band of the marker can be observed the over-expression of Hcen2.

## Isolation and Purification of Human centrin 1 and 2

### *Affinity Chromatography using Phenyl Sepharose CL-4B column.*

The protocol used to isolate and purify the human centrin isoforms *was* similar to that established in the laboratory for *Chlamydomonas* centrin (Pastrana, et. al. 2002). The harvested cells were lysed and centrifuged. The resulting supernatant was loaded in to a CL-4B (Sigma, St Louis, MO) column. The characteristic chromatogram was obtained for both human isoforms (Hcen1 and Hcen2) where two distinctive peaks can be observed. Peak A, corresponds to elution of low affinity *E. coli* proteins, that is, those proteins that do not interact with the column matrix in the presence of low salt and cation concentration. Peak B corresponds to centrin elution upon removal of calcium by EGTA (Figure 18). Here is reported the elution profile of Hcen1 and for Hcen2 (*data not shown*).

The fractions collected through affinity chromatography time course were analyzed by microfluidic Lab-chip electrophoresis from Agilent Technologies (Figure 19 and 20). For Hcen1 the fractions collected and analyzed are shown in Figure 19. The proteins eluted in the void volume, that did not interact with the column matrix are shown in the lane titled void A. In the lanes titled fractions 32 – 57 (Fr 32 to Fr 57) are fractions that contain the protein of interest (MrW 21.5 kDa). This band (MrW 21.5 kDa) corresponds to Hcen1 elution during the peak B from chromatogram. The profile of elution peak B can be also observed in the lab chip electrophoresis gel. Furthermore, a smaller Hcen1 concentration in the void C lane confirms this profile.

Similar results were obtained for Hcen2 affinity chromatography elution profile (Figure 20). In the void A lane elution of non interacting proteins (*E. coli*) can be observed. In the lanes entitled fractions B1 – B (Frac B1 to Frac B) are fractions that contain the protein of interest (MrW 21.5 kDa). This band (MrW 21.5 kDa) corresponds to Hcen2 elution during the peak B from chromatogram.

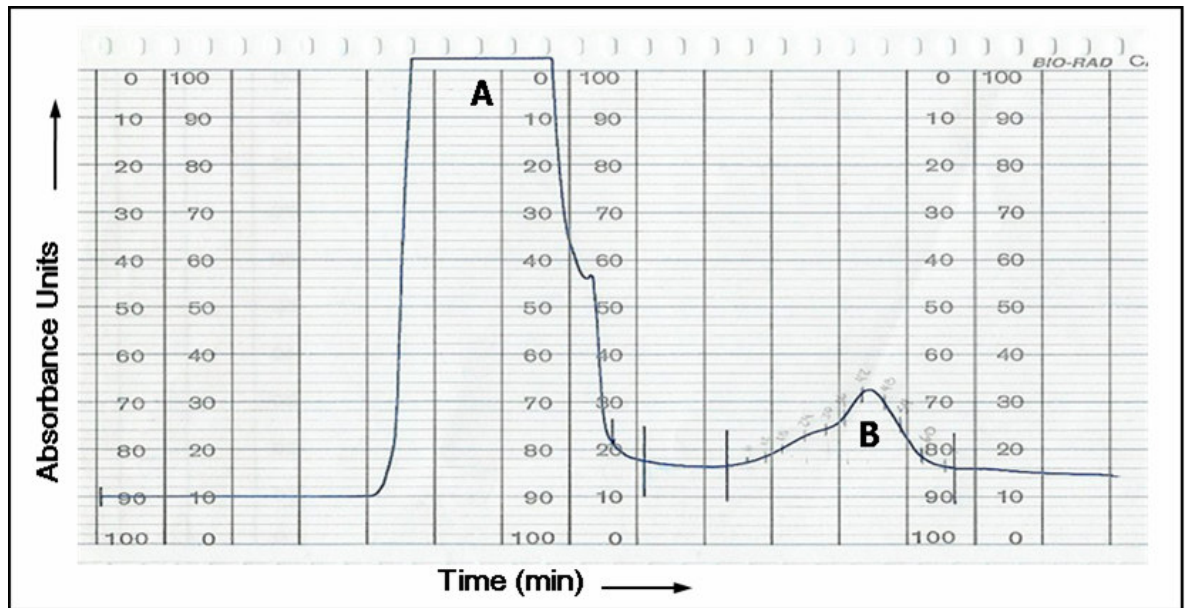


**Figure 18. Phenyl Sepharose chromatogram**

Elution profile characteristic of Hcen1 through Phenyl Sepharose column. (A) Elution of low affinity proteins which not interact with the matrix. (B) Elution of centrin proteins and proteins that had similar centrin interaction with the matrix. Vertical lines are points during the chromatographic run where the eluent was changed.

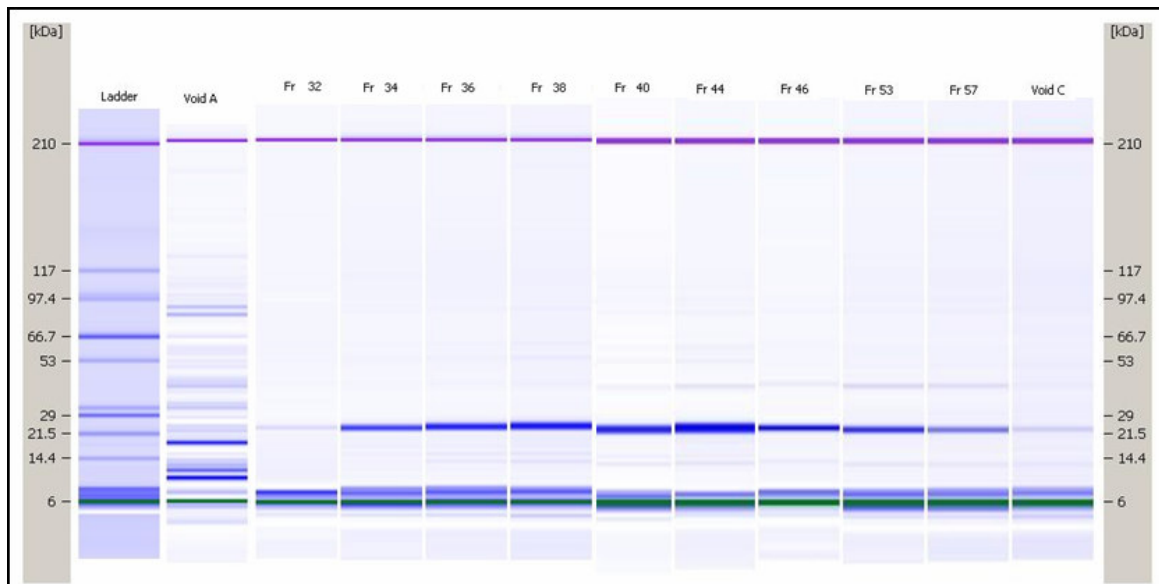


**Figure 19. Lab chip electrophoresis gel from Hcen 1 affinity chromatography.**

Microfluidic Lab-chip electrophoresis of fractions collected during Hcen1 affinity chromatography. The fractions from 32 to 57 where a band with MrW to 21.5 kDa is observed correspond to Hcen1 elution within peak B of the affinity chromatogram.

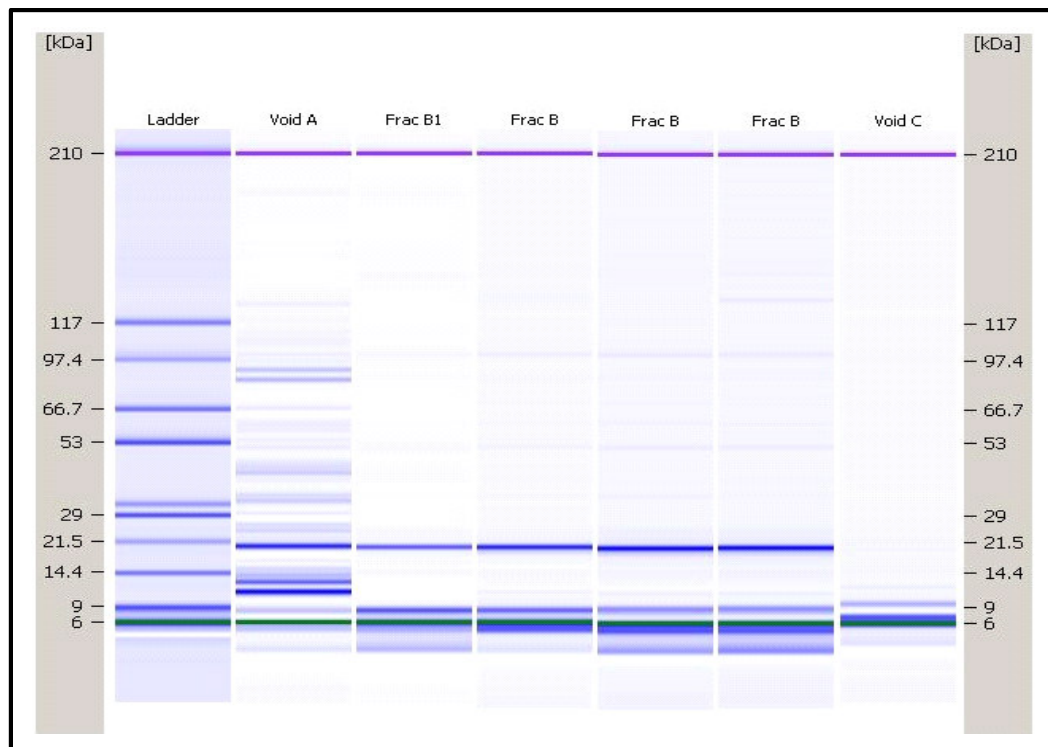


**Figure 20. Lab chip electrophoresis gel from Hcen 2 affinity chromatography.**

Microfluidic Lab-chip electrophoresis of fractions collected during Hcen2 affinity chromatography. The fractions from B1 and B where a band with MrW to 21.5 kDa is observed correspond to Hcen2 elution within peak B of the affinity chromatogram.

### ***Anion Exchange Chromatography***

The fractions identified containing centrin were pooled, concentrated, buffer exchanged and subjected to an anion exchange column. The centrin elution was achieved using a NaCl gradient from 0 to 0.75 N and monitored at 280 nm. Figure 21 shows the typical centrin chromatogram profile that was obtained for Hcen1 and Hcen2 in this step. Peak A corresponds to the elution of cationic proteins, those that did not interact with the matrix column. The elution of centrin according to increase from 0 to 0.75 N NaCl gradient can be observed in peaks B and C. The peak D corresponds to other bacterial proteins that elute at 1 N NaCl.

The fractions collected from centrin elution were analyzed by microfluidic Lab chip electrophoresis. In lab chip electrophoresis gel, the band at MrW 21.5 kDa can be observed for Hcen1 in the Figure 22A and Figure 22B for Hcen2. A purity >98 % for Hcen1 and Hcen2 was obtained.

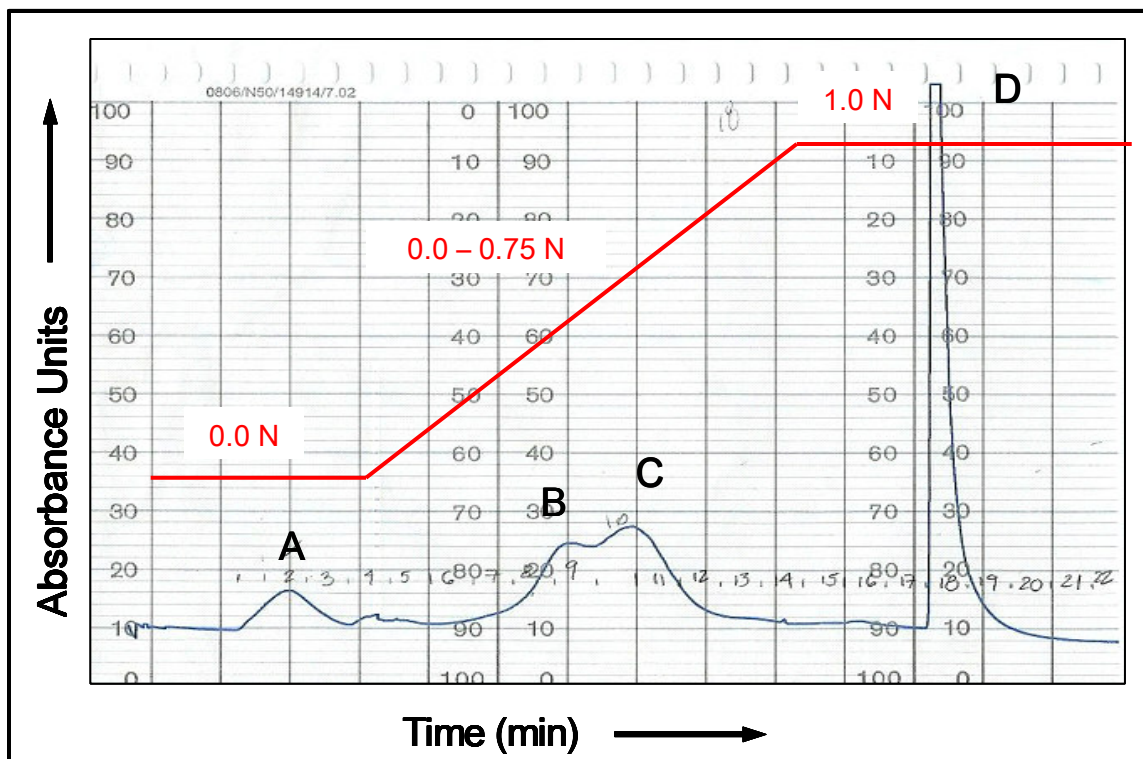


**Figure 21. Anion exchange chromatogram.**

Typical chromatogram obtained from elution of Hcen1 and Hcen2 through anion exchange column. (A) Elution of proteins that did not interact with the matrix column, (B and C) elution of centrin and (D) elution of other proteins

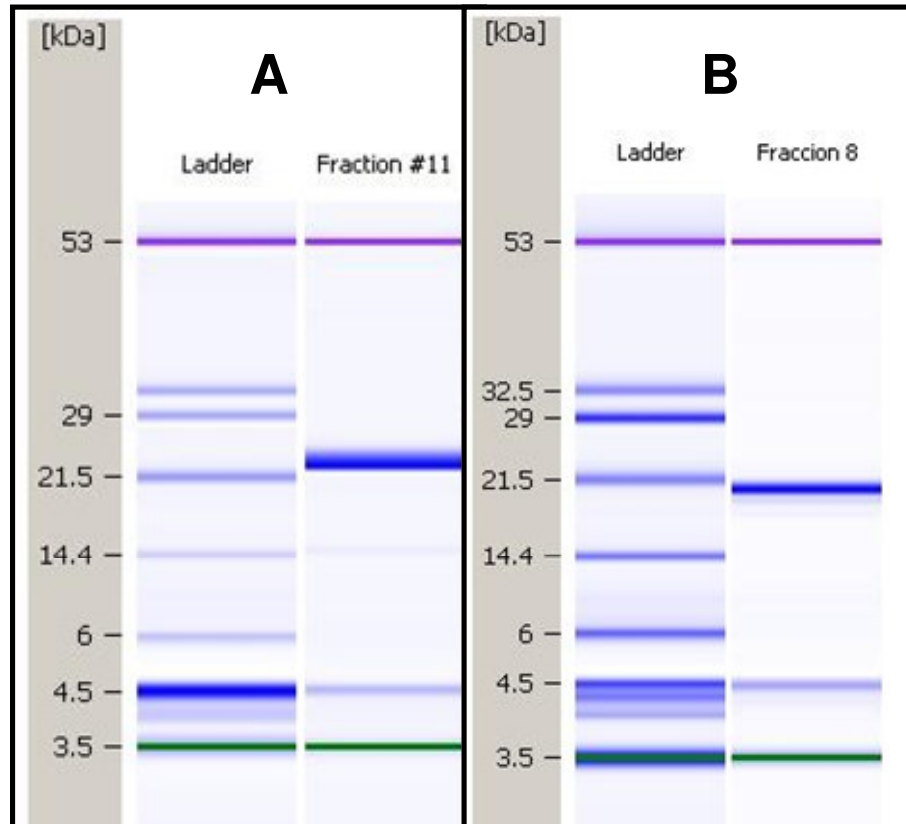


**Figure 22. Lab chip electrophoresis gel from Hcen 1 and Hcen 2 anion exchange chromatography.**

(A) Ladder lane and Hcen1 >98% pure, and (B) Ladder lane and Hcen2 >98% pure. In the sample lane the other band also observed is the internal standard at MrW 4.5 Da.

### *UV Spectroscopy Assays*

The pure centrin fractions obtained after anion exchange chromatography were pooled and concentrated. The purified centrin was subjected to UV analysis and a spectrum from 245 to 320 nm region was acquired (Figure 23). The spectrum show the three characteristics peaks of phenylalanine (252, 259 and 265 nm) with maximum absorbance at 259 nm and a distinct tyrosine peak at 280 nm (see figure 3). The absence of 290 nm tryptophan peak confirmed the purity of human centrin proteins. To determine the protein concentration was necessary the molar extinction coefficient ( $\epsilon$ ) calculation, as described in the following equation (Creighton. Proteins, 2nd edition):

$$\epsilon_{280 \text{ nm}} = (n \text{ Trp} \times 5540) + (n \text{ Tyr} \times 1480) + (n \text{ Cystine} \times 156) + (n \text{ Phe} \times 5) \quad (11)$$

where  $n$  is the number of each residue type in the protein sequence (see Scheme 1) and the stated values are the amino acid molar extinction coefficient at 280 nm. The calculated molar extinction coefficient for both human isoforms is  $1,530 \text{ M}^{-1} \text{ cm}^{-1}$ ; since they contain ten phenylalanine residues and one tyrosine residue within its sequence. Solving the expression for Beer and Lambert

$$A = \epsilon b c \quad (12)$$

where A is the absorbance in arbitrary units,  $\epsilon$  is the molar extinction coefficient of the desire protein ( $1530 \text{ M}^{-1} \text{ cm}^{-1}$ ), b is the pathlength (1 cm), and c is the molar concentration (M). Consequently, the protein yields were 14.8 mg for Hcen1 and 11.14 mg for Hcen2.

### ***Mass Spectrometry***

The purity, integrity and molecular weight were verified by MALDI-TOF mass spectrometry at the MS facility at Vanderbilt University. The calculated molecular weight for Hcen1 is 19,570 Da while the experimental value obtained was a parent peak at 19,419 m/z possibly due to non specific protein cleavage of Met<sub>1</sub> and the loss of one magnesium cation (Figure 24). For Hcen2 the calculated molecular weight is 19,738 Da while the experimental mass to charge ratio was 19,698 m/z due to the loss of one calcium cation (Figure 25).

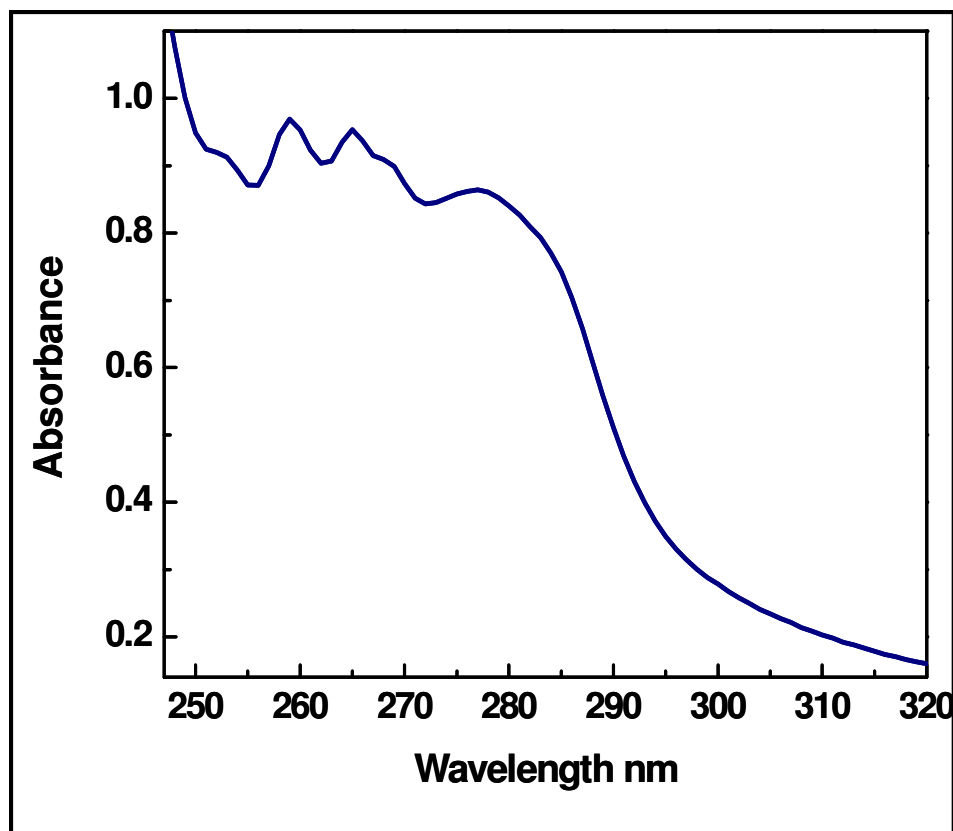


**Figure 23. UV spectrum of pure Hcen1 (similarly for Hcen 2)**

The characteristic three phenylalanine peaks with  $\lambda_{\max}$  at 252, 259 and 265 nm and tyrosine absorbance at 280 nm can be observed.

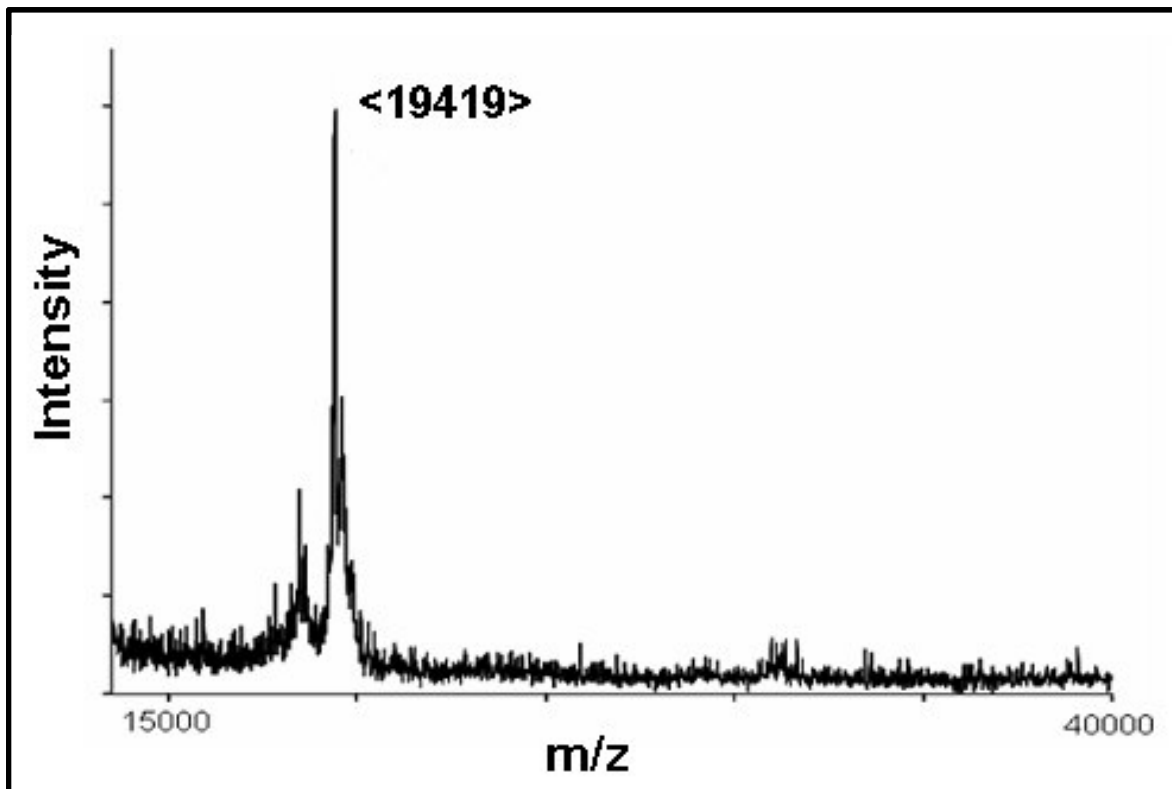


**Figure 24. MALDI-TOF MS spectrum of Hcen1.**

The mass/charge ratio peak is consistent with the calculated molecular weight. Thus, the protein integrity and purity was confirmed.

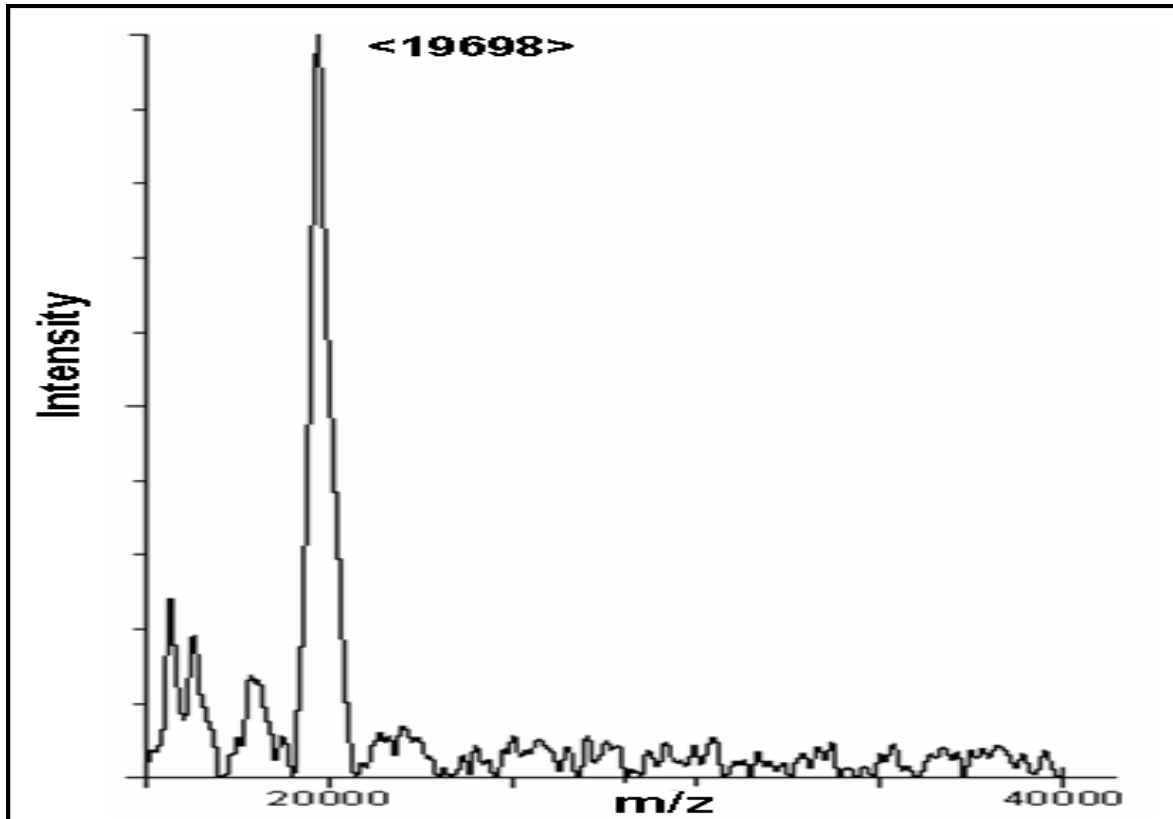


**Figure 25. MALDI-TOF MS spectrum of Hcen2.**

The mass/charge ratio peak is consistent with the calculated molecular weight. Thus, the protein integrity and purity was confirmed..

## FT-IR Spectroscopy

FT-IR spectra were obtained for Hcen1 and Hcen2 as a function of temperature (0.5 – 88 °C) in the presence of calcium. The spectral changes in the spectral region 1700-1530  $\text{cm}^{-1}$  were closely monitored during the thermal perturbation. These spectral changes were studied in detail by curve fitting analysis, difference spectroscopy and 2DCOS analysis. The overlaid spectra acquired for Hcen1 and Hcen2 is shown in figure 26A and 26B, respectively. Although the proteins were fully H→D exchanged prior to the perturbation the amide II presence is evident in the spectra, because of the overlapping absorbance of certain side chain vibrational modes, mainly aspartate, glutamate, and arginine which account for 29% of the Hcen1 sequence and 27% of the Hcen2 sequence. Superposition of initial and final spectrum acquired from Hcen1 and Hcen2 thermal perturbation showed that for Hcen1 the amide I' band is shifted from 1642  $\text{cm}^{-1}$  to 1648  $\text{cm}^{-1}$ , while the side chain band is shifted from 1575  $\text{cm}^{-1}$  to 1577  $\text{cm}^{-1}$  as shown in figure 26C. For Hcen2 the contribution amide I' band (1647  $\text{cm}^{-1}$ ) is slightly decreased while the contribution of the amide II band (1579  $\text{cm}^{-1}$ ) increased through the thermal perturbation as can be observed in figure 26D.

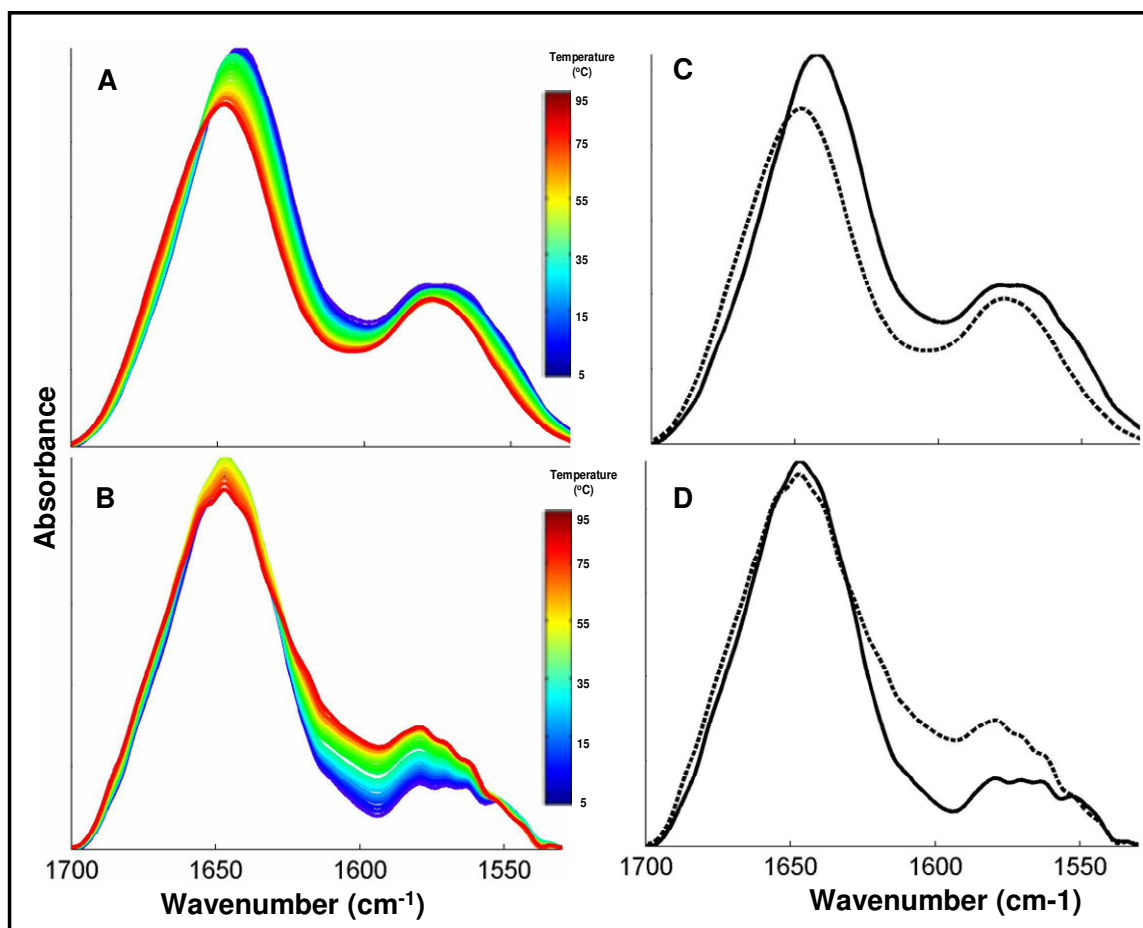


**Figure 26. FT-IR overlay spectra.**

FT-IR overlay of (A) Hcen1 and (B) Hcen2 in the 1700-1530 cm<sup>-1</sup> spectral region. The side colors bar shows the color correspondence with temperature. The Hcen1 (C) and Hcen2 (D) overlay of initial (solid line) and final (dashed line) spectrum obtained from thermal perturbation. For Hcen1 the amide I' band is shifted by 6 cm<sup>-1</sup> (1642 - 1648 cm<sup>-1</sup>) and the side chain band is shifted by 2 cm<sup>-1</sup> (1575 - 1577 cm<sup>-1</sup>). For Hcen2 the amide I' band (1647 cm<sup>-1</sup>) contribution decrease lightly while the side chain band (1579 cm<sup>-1</sup>) contribution increased.

Difference spectra were generated by subtracting the first spectrum from all subsequent spectra for the spectral region of 1700-1530  $\text{cm}^{-1}$ . The peak assignment for the maxima (+) or minima (-) resulting from an increase or decrease in overall peaks is summarized as follows. For Hcen1 the peak assignments are comprised of  $\beta$ -turns ((+) 1667 $\text{cm}^{-1}$ ), random coil ((+) 1662  $\text{cm}^{-1}$ ),  $3_{10}$ -helix ((+) 1650  $\text{cm}^{-1}$  and become (-) after 36°C),  $\beta$ -stand ((-) 1630  $\text{cm}^{-1}$ ), arginine side chain modes ((+) 1590 and 1611  $\text{cm}^{-1}$ ), and glutamate side chain modes ((-) 1555  $\text{cm}^{-1}$ ) as shown in figure 27A. The resulting difference spectra for Hcen2, the peak assignments are comprised of loops ((+) 1682  $\text{cm}^{-1}$ ),  $\beta$ -turns ((+) 1677  $\text{cm}^{-1}$ ),  $\alpha$ -helix ((+) 1646  $\text{cm}^{-1}$  and become (-) after 58°C),  $\beta$ -sheets ((+) 1630  $\text{cm}^{-1}$  and become (-) after 58°C), arginine side chain modes ((+) 1594 and 1581  $\text{cm}^{-1}$ ), and aspartate side chain modes ((+) 1569  $\text{cm}^{-1}$ ) as shown in figure 27B.

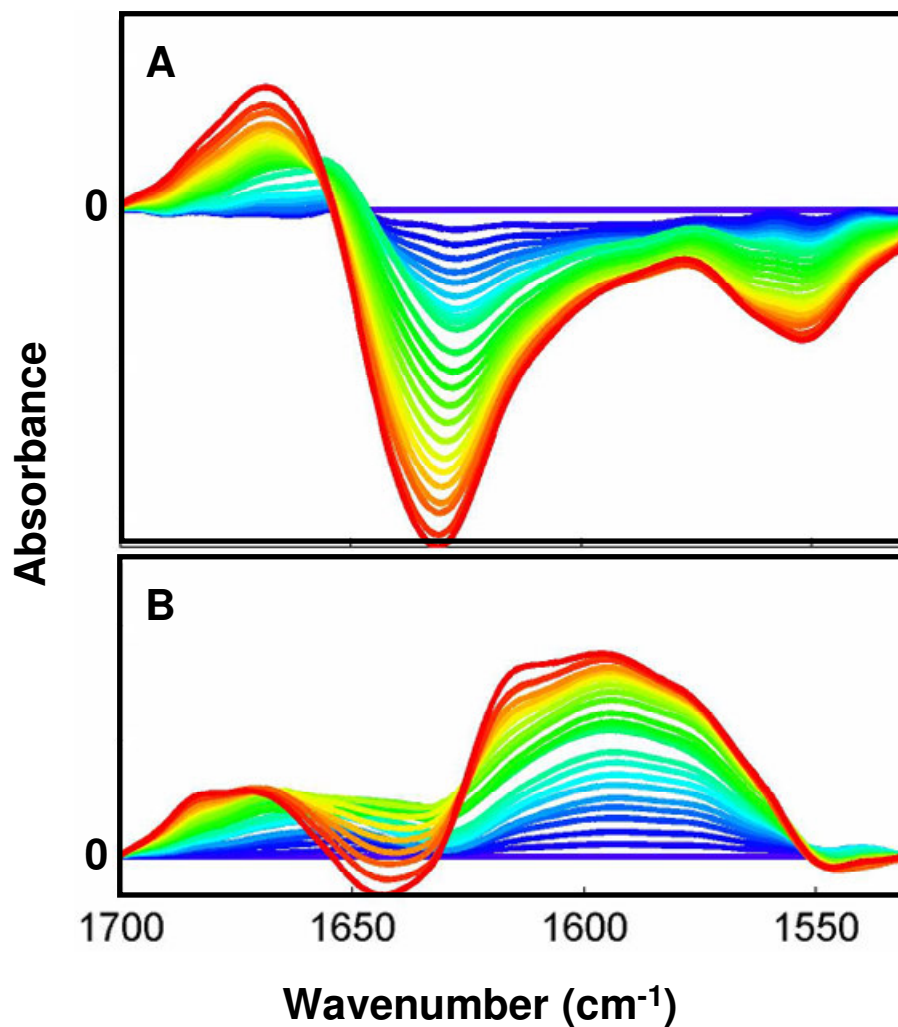


**Figure 27. Overlaid difference spectra of Hcen (A) and Hcen2 (B) within spectral region 1700 – 1530  $\text{cm}^{-1}$ .**

The difference spectra were generated by subtraction of the first spectrum from all subsequent spectra.

## Curve-fitting analysis

The curve-fitting analysis was performed for the secondary structure determination of Hcen1 and Hcen2 at 20°C (Figure 28). For the spectral curve fitting, a series of subband assignments were made for simulation of the experimental spectra. The position and number of subbands used were determined from the FT-IR 2D-correlation analysis (discussed below). The results were compared with the available high resolution structural data as summarized in Table 4. For Hcen2 the percent secondary structure contributions were 17.1 %  $\beta$ -sheets, 20.6 % random coil, 51.6 %  $\alpha$ -helix and 10.7 %  $\beta$ -turns which is in good agreement with the available X-ray crystallographic data for Hcen2-XPC complex (PDB: 2GGM) at 20°C (Thompson, et. al. 2006). The Hcen2 results for random coil,  $\alpha$ -helix and  $\beta$ -turns. Disagreement is observed within the  $\beta$ -sheets (17.1% and 5%, FT-IR and X-ray, respectively), and there was no discrimination made between the  $\alpha$ - and  $3_{10}$ -helical components in centrin by FT-IR curve fitting, also the discrepancy may be due to the presence of XPC peptide or the lack of the first 24 residues in the structural data reported. For Hcen1, there is no high resolution structural data available. Therefore, the secondary structure results presented herein for Hcen1 are comprised of 17.7 %  $\beta$ -sheets, 15.62 % random coil, 59.4 %  $\alpha$ -helix and 7.3 %  $\beta$ -turns. The results obtained are consistent with one another.

Table 4. Summary of the percent secondary structure for Hcen1 and Hcen2

Protein	Percent Secondary Structure					Method
	$\alpha$ -helix	$\beta$ -sheets	$3_{10}$ helix	rc	$\beta$ -turn	
Hcen1	----- 59.4	----- 17.7	----- ----- <sup>b</sup>	----- 15.6	----- 7.3	None <sup>a</sup> IR
Hcen2	52 51.6	5 17.1	2 ----- <sup>b</sup>	23 20.6	7 10.7	X-ray <sup>c</sup> IR

<sup>a</sup>Data not available, <sup>b</sup> data not determined by IR spectroscopy and <sup>c</sup> data acquired from PDB:2GGM.

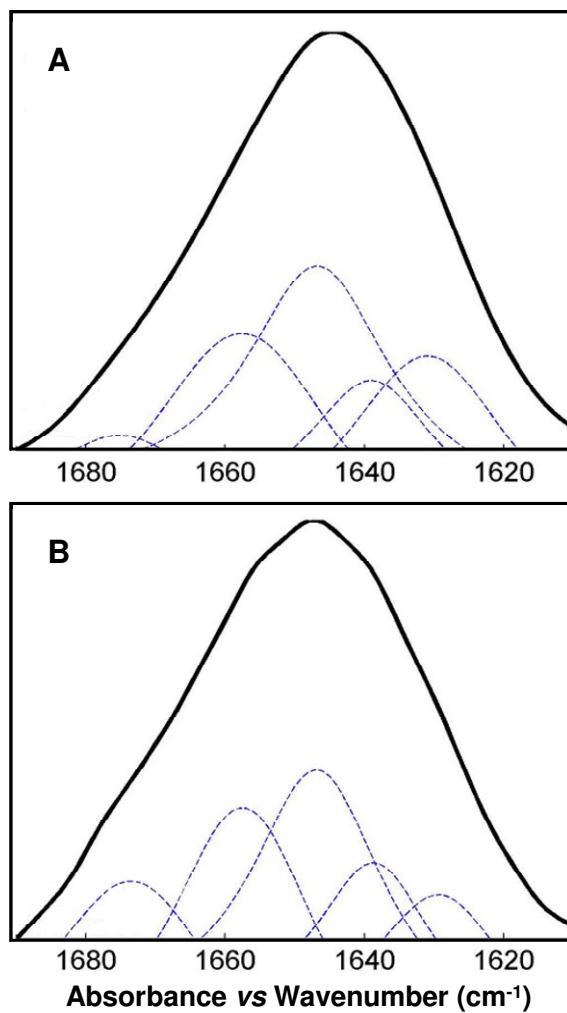


**Figure 28. Curve fitted FT-IR spectra of Hcen1 and Hcen2.**

Solid lines are the experimental spectrum and dotted line are the contributing subbands for Hcen1 (A) and Hcen2 (B) in spectral region of 1700 – 1600 cm<sup>-1</sup> at 20 °C.

## Two-dimensional correlation analysis

The acquired FT-IR spectra were studied using two-dimensional correlation analysis, in order to enhance the spectral resolution, extract correlation and information about thermal stability of Hcen1 and Hcen2 from the spectral changes that occur during the thermal perturbation. Each data set was analyzed within the spectral region of 1700 – 1530  $\text{cm}^{-1}$ . Two different plots were obtained for Hcen1 and Hcen2, the synchronous plots, which reflect in-phase transitions are shown in figure 29A and 29B, and the asynchronous plots, which reflect out-of-phase transitions, are shown in figure 28C and 28D.

### *Synchronous plots*

In these plots we can observe diagonal peaks which are called positive auto peaks and these are peaks that correspond to vibrational modes that are being perturbed by temperature. The off diagonal peaks observed known as cross peaks, reflect the correlation of the auto peaks that are being perturbed. The auto peaks assignment is summarized in Table 5 for Hcen1 and Hcen2.

The synchronous plot for Hcen1 show in Figure 29A three main auto peaks at 1672  $\text{cm}^{-1}$  ( $\beta$ -turns), 1630  $\text{cm}^{-1}$  ( $\beta$ -sheets) and 1555  $\text{cm}^{-1}$  (glutamate), where the strongest intensity change is observed for 1630  $\text{cm}^{-1}$  ( $\beta$ -sheets) with three underlying contributions at 1647  $\text{cm}^{-1}$  assigned to  $\alpha$ -helix, 1611  $\text{cm}^{-1}$  and 1590  $\text{cm}^{-1}$  assigned to arginine side chain

modes. These underlying contributions are confirmed by cross peaks correlations within the same plot. (Figure 29C).

For Hcen2 the synchronous plot (Figure 29B) shows three main auto peaks summarized in Table 5. These auto peaks are at  $1581\text{ cm}^{-1}$  and  $1597\text{ cm}^{-1}$  (arginine symmetric and asymmetric stretch, respectively). The third auto peak corresponds to  $1619\text{ cm}^{-1}$  which is due to self association or aggregation. The positive cross peaks presence correlation shows that the changes in arginine ( $1597$  and  $1581\text{ cm}^{-1}$ ) are correlated with loops ( $1683\text{ cm}^{-1}$ ) and  $\beta$ -turns ( $1672\text{ cm}^{-1}$ ).

### ***Asynchronous plots***

The asynchronous plots are quite different from the synchronous plot; here the color of the cross peaks, as well as their counterparts in the synchronous plots, allow the determination of the order of events during the thermal perturbation. This order is summarized in the Table 5. Also, the existence of auto peaks observed in the synchronous plot is confirmed by asynchronous plot.

In Figure 29C for Hcen1, the positive cross peaks (red):  $\alpha$ -helix ( $1647\text{ cm}^{-1}$ ), and  $\beta$ -sheets ( $1628\text{ cm}^{-1}$ ) are observed to correlate with  $\beta$ -turns ( $1675\text{ cm}^{-1}$ ) and glutamate ( $1557\text{ cm}^{-1}$ ). Negative correlating peaks (blue) are  $\beta$ -turns ( $1675\text{ cm}^{-1}$ ) correlating with  $\alpha$ -helix ( $1647\text{ cm}^{-1}$ ),  $\beta$ -sheets ( $1628\text{ cm}^{-1}$ ), and glutamate ( $1557\text{ cm}^{-1}$ ). This way, the order of events throughout the thermal perturbation is detailed as follows:  $\alpha$ -helix followed by  $\beta$ -sheets then glutamate and finally  $\beta$ -turns.

For Hcen2 (Figure 29D) a significant negative cross peaks:  $\alpha$ -helix ( $1647\text{ cm}^{-1}$ ) and  $\beta$ -sheets ( $1633\text{ cm}^{-1}$ ) are observed to correlate with self association or aggregation ( $1619\text{ cm}^{-1}$ ) and arginine side chains modes ( $1594$  and  $1579\text{ cm}^{-1}$ ). The positive correlating cross peaks are loops ( $1685\text{ cm}^{-1}$ ),  $\beta$ -turns ( $1674\text{ cm}^{-1}$ ) and self association or aggregation ( $1619\text{ cm}^{-1}$ ) with ( $\alpha$ -helix ( $1647\text{ cm}^{-1}$ ) and arginine ( $1594$  and  $1579\text{ cm}^{-1}$ ). Thus, the order of events for the entire temperature range is then as follows:  $\alpha$ -helix followed by aggregation, then  $\beta$ -turns arginine and finally loops.

Table 5. Summary of peak assignment obtained from synchronous and asynchronous plots for Human centrin 1 and Human centrin 2.

Assignment	Human centrin 1		Human centrin 2	
	Synchronous Auto Peaks (cm <sup>-1</sup> )	Asynchronous Cross Peaks (cm <sup>-1</sup> )	Synchronous Auto Peaks (cm <sup>-1</sup> )	Asynchronous Cross Peaks (cm <sup>-1</sup> )
Loops	----	----	1683	1685
β-turns	1672	1675	1672	1674
α-helix	1647	1647	1647	1646
Aggregation	----	----	1619	1619
β-sheets	1630	1628	----	----
Arginine (Arg)	----	----	1597, 1581	1594, 1579
Glutamate (Glu <sup>-</sup> )	1555	1557	---	---

---- Not observed.

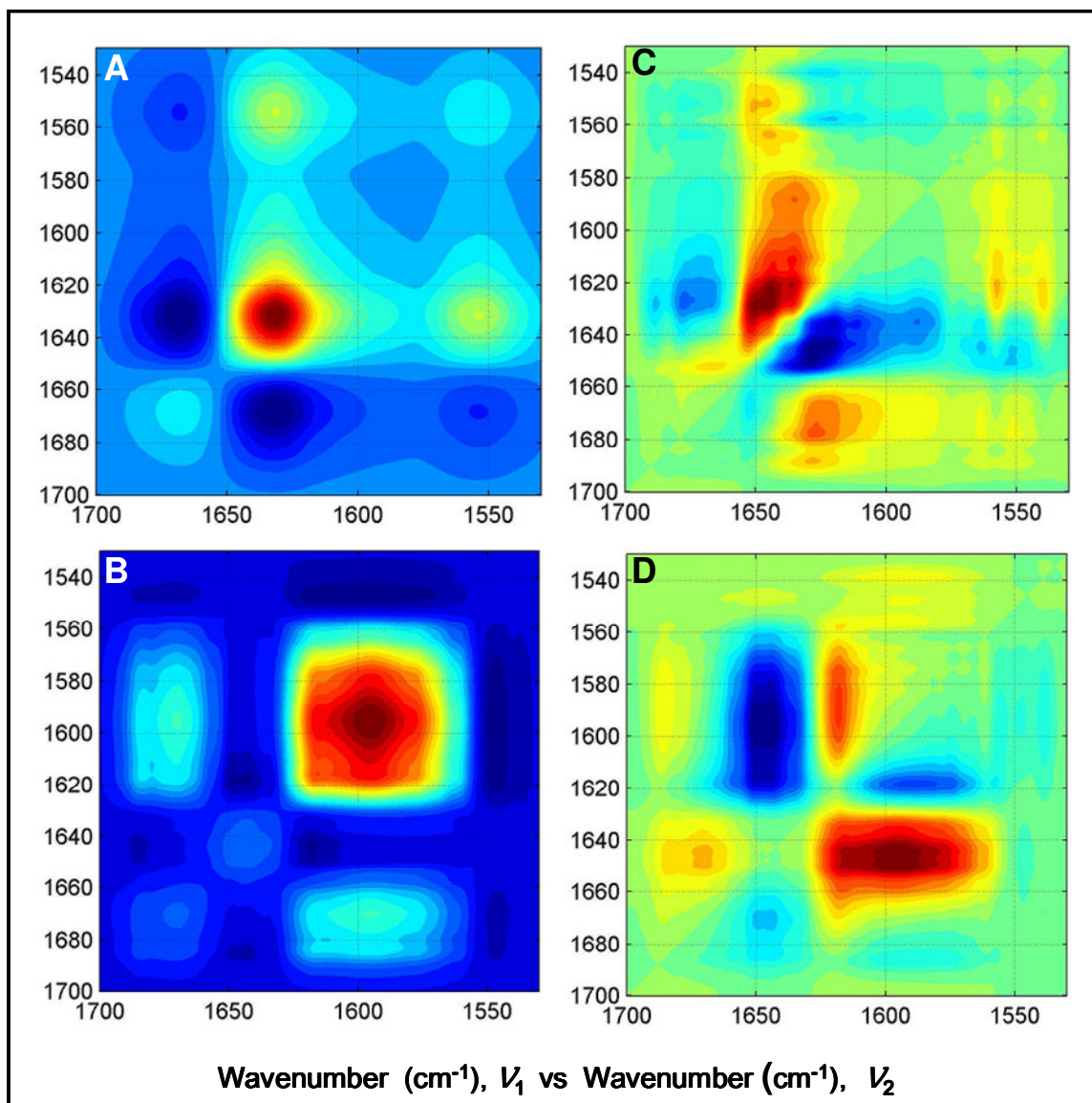


**Figure 29. Synchronous and asynchronous contour plots in the spectral region of 1700 – 1530 cm<sup>-1</sup>.**

For H cen1 (A and C) and Hcen2 (B, and D).

Table 6. Summary of phase analysis of the asynchronous plot used to determine the order of events during thermal perturbation for: Hcen1 and Hcen2.

Event	Order of Events *
<b>Hcen1</b>	
1	$\alpha$ -helix (1647 $\text{cm}^{-1}$ ) prior to $\beta$ -sheets (1630 $\text{cm}^{-1}$ )
2	$\beta$ -sheets (1630 $\text{cm}^{-1}$ ) prior to Glu <sup>-</sup> (1555 $\text{cm}^{-1}$ )
3	Glu <sup>-</sup> (1555 $\text{cm}^{-1}$ ) prior to $\beta$ -turn (1672 $\text{cm}^{-1}$ )
4	$\beta$ -sheets (1630 $\text{cm}^{-1}$ ) prior to $\beta$ -turn (1672 $\text{cm}^{-1}$ )
<b>Hcen2</b>	
1	$\alpha$ -helix (1646 $\text{cm}^{-1}$ ) prior to aggregation (1619 $\text{cm}^{-1}$ )
2	aggregation (1619 $\text{cm}^{-1}$ ) prior to $\beta$ -turn (1672 $\text{cm}^{-1}$ )
3	$\beta$ -turn (1672 $\text{cm}^{-1}$ ) prior to Arg (1594, 1579 $\text{cm}^{-1}$ )
4	Arg (1594, 1579 $\text{cm}^{-1}$ ) prior to loop (1683 $\text{cm}^{-1}$ )

\* Sequence of spectral intensity changes in ascending order of temperature.

### **Thermal dependence study**

The FT-IR amide I' band position was monitored during the thermal perturbation from 0.5 °C to 88 °C. We plotted the amide I band maximum vs temperature for Hcen1 and Hcen2 as shown in Figure 30. A pretransition was observed at 1.7 – 4.8 °C and the onset of the final transition temperature was observed between 80.5 – 84 °C for Hcen1 (Figure 30A). For Hcen2 the thermal dependence profile (Figure 30B) is different when compare to Hcen1. To determine the events that occur during Hcen2 thermal dependence study the spectral data acquired was separated in five data sets according to the thermal dependence profile (see 2DCOS temperature induced changes in Hcen2).

The spectral data was divided into several temperature ranges to provide a more detailed description of the molecular events that occurred during thermal dependence perturbation of Hcen2 (see figure 29): (1) initial temperature range (2 - 16 °C), (2) second temperature range (16 - 28 °C), (3) third temperature range (28 - 43 °C), (4) fourth temperature range (43 - 58 °C) and (5) final temperature range (58 to 77 °C).

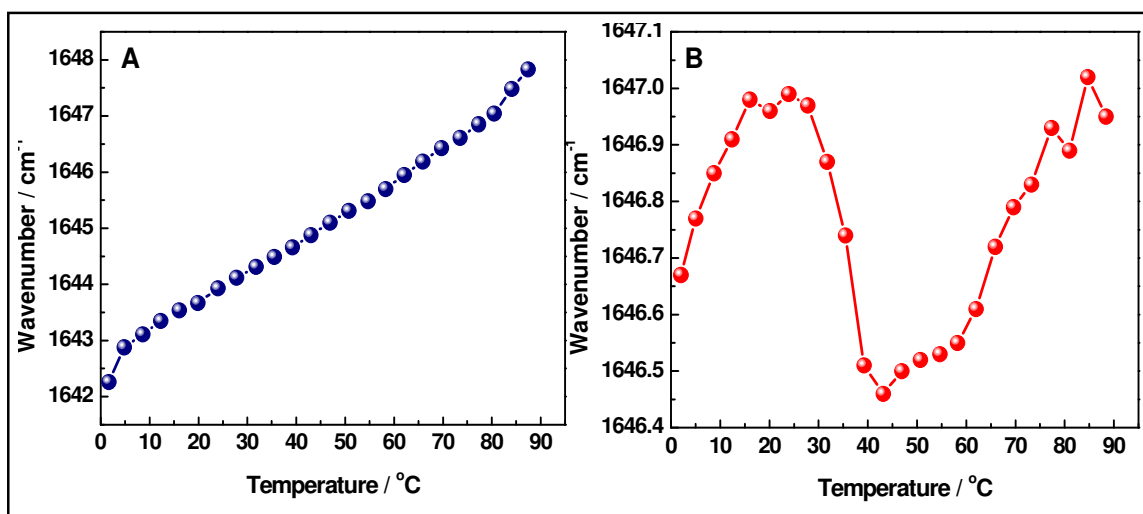


**Figure 30. Thermal dependence study for Hcen1(A) and Hcen2 (B)**

Two pre transition points (around 2 and 82 °C) can be observed to Hcen1. A different behavior was observed to Hcen2.

## Two-dimensional correlation analysis: a detailed description of temperature induced changes in Hcen2

We obtained an in-depth description of the secondary structure and side chains modes vibrational changes that occur throughout the thermal perturbation profile for Hcen2. Small spectral data sets in the region of 1700 – 1530  $\text{cm}^{-1}$  were used and generated several 2DCOS plots to provide a detailed description of the order of events for Hcen2. Auto peaks positions determined from the synchronous plots (Figures 31A, 31B, 32E, 32F and 33I) and correlation peaks determined from the asynchronous plots (Figures 31C, 31D, 32G, 32H and 33J) for each data set of thermal dependence study are summarized in Table 7. These band assignments and positions were used to describe the changes observed for Hcen2 that are summarized in the Table 8.

During the first temperature range (2 – 18 °C), the synchronous (Figure 31A) and asynchronous (Figure 31C) plot show that arginine (1590, 1575  $\text{cm}^{-1}$ ) was affected by thermal perturbation prior to  $3_{10}$ -helix (1650  $\text{cm}^{-1}$ ) followed by aspartate (1560  $\text{cm}^{-1}$ ) and glutamate (1540  $\text{cm}^{-1}$ ) and finally the loops (1683  $\text{cm}^{-1}$ ). For this temperature range the strongest intensity changes were observed for arginine side chain modes (1590, 1575  $\text{cm}^{-1}$ ).

The thermal dependence plot suggests minimal changes for Hcen2 within temperature range from 16 to 28 °C. The synchronous (Figure 31B) and asynchronous (Figure 31D) plot analysis show arginine (1594, 1581  $\text{cm}^{-1}$ ) with biggest intensity changes in this range. The order of events are:  $3_{10}$ -helix (1653  $\text{cm}^{-1}$ ) prior to random coil (1663  $\text{cm}^{-1}$ ), followed by arginine side chains modes (1594, 1581  $\text{cm}^{-1}$ ) and finally loops (1682  $\text{cm}^{-1}$ ).

The synchronous (Figure 32E) and asynchronous (Figure 32G) plot for 28 – 43 °C temperature range of Hcen2 thermal dependence study the strongest intensity changes can be observed for arginine (1600, 1581  $\text{cm}^{-1}$ ) with  $\alpha$ -helix (1644  $\text{cm}^{-1}$ ) subjacent contribution. The auto peak at 1644  $\text{cm}^{-1}$  is due to contribution of a less exposed  $\alpha$ -helix suggesting a conformational change in the protein. This is according with the downward tendency in the thermal dependence plot (Figure 30B). The more exposed  $3_{10}$ -helix (1650  $\text{cm}^{-1}$ ) and less exposed  $\alpha$ -helix (1644  $\text{cm}^{-1}$ ) contribution has also been determined previously for *Chlamydomonas* centrin (Ortiz, et. al. 2005 and Sanoguet, et. al. 2006). The more exposed  $3_{10}$ -helix has been located in the C-terminal domain which binds to its biological target peptide (Ortiz, et. al. 2005, Kilmartin, et. al. 2006 and Thompson, et. al. 2006). Therefore, the order of events in this range are as follows: glutamate (1544  $\text{cm}^{-1}$ ), random coil (1668  $\text{cm}^{-1}$ ) followed by arginine (1600, 1581  $\text{cm}^{-1}$ ), then  $\alpha$ -helix (1644  $\text{cm}^{-1}$ ) and finally loops (1688  $\text{cm}^{-1}$ ).

For the data set corresponding to 43 to 58 °C of the thermal dependence profile (Figure 30), the synchronous (Figure 32F) and asynchronous (Figure 32H) plots show the biggest intensity changes occurring for arginine (1594, 1575  $\text{cm}^{-1}$ ). It is at this temperature range that the appearance of an auto peak at 1619  $\text{cm}^{-1}$  assigned to aggregation can also be observed in the synchronous plot and is confirmed as a cross peak in the asynchronous plot. The aggregation assignment was previously reported by Pastrana et. al. 2002. The order of events for this temperature range can then be summarized as glutamate (1540  $\text{cm}^{-1}$ ),  $3_{10}$ -helix (1653  $\text{cm}^{-1}$ ) prior to random coil (1669  $\text{cm}^{-1}$ ) followed by aggregation (1619  $\text{cm}^{-1}$ ) then arginine (1594, 1575  $\text{cm}^{-1}$ ), and finally the loops (1684  $\text{cm}^{-1}$ ).

In the temperature range of 58 – 77 °C the thermal dependence profile the strongest intensity change observed is the  $\alpha$ -helix (1645  $\text{cm}^{-1}$ ). In the synchronous plot (Figure 33I) two main auto peaks can be observed at 1645  $\text{cm}^{-1}$  ( $\alpha$ -helix) and 1619  $\text{cm}^{-1}$  (aggregation) with underlying contribution of arginine (1596, 1581  $\text{cm}^{-1}$ ). A weaker auto peak can also be observed at 1684  $\text{cm}^{-1}$  (loops). The negative cross peaks correlate the  $\alpha$ -helix (1645  $\text{cm}^{-1}$ ) with the loops (1684  $\text{cm}^{-1}$ ) and aggregation (1619  $\text{cm}^{-1}$ ) suggesting that these events are out of phase coupled.

From the asynchronous plot, cross peaks shown in Figure 33J were used to determine the order of events as follows: arginine (1596, 1581  $\text{cm}^{-1}$ ), then  $3_{10}$ -helix (1650  $\text{cm}^{-1}$ ) followed by aspartate/glutamate (1560 / 1540  $\text{cm}^{-1}$ ), then random coil (1669  $\text{cm}^{-1}$ ),  $\alpha$ -helix (1645  $\text{cm}^{-1}$ ), followed by aggregation (1619  $\text{cm}^{-1}$ ), and finally loops (1683  $\text{cm}^{-1}$ ).

Table 7. Summary of peak assignment obtained from synchronous and asynchronous plots for each data set from Hcen2 thermal dependence study

Assignment	2 – 16 °C		16 – 28 °C		28 – 43 °C		43 – 58 °C		58 – 77 °C	
	Sync*	Async**	Sync	Async	Sync	Async	Sync	Async	Sync	Async
	Auto	Cross								
	Peaks (cm <sup>-1</sup> )									
Loops	1683	1685	1682	1682	1688	1690	1684	1687	1684	1684
Random coil	----	----	1663	1665	1668	1668	1669	1672	----	----
α-helix	1650	1650	1653	1650	1644	1647	1653	1656	1645	1644
Aggregation	----	----	----	----	----	----	1619	1622	1619	1619
Arginine (Arg)	1590 / 1575	1590 / 1575	1594 / 1581	1600 / 1584	1600 / 1581	1600 / 1581	1594 / 1575	1600 / 1581	1596 / 1581	1594 / 1575
Aspartate (Asp)	1560	1557	----	----	----	----	----	----	----	----
Glutamate (Glu)	1540	1541	---	---	1544	1541	1540	1540	---	---

\*Sync: Synchronous and \*\*Async: Asynchronous.

---- Not observed.

**Table 8. Summary of phase analysis of the asynchronous plots used to determine dynamics during the thermal dependence study of Hcen2.**

Event	Order of Events *
<b>2 – 16 °C</b>	
1	Arg (1590, 1575 cm <sup>-1</sup> ) prior to 3 <sub>10</sub> -helix (1650 cm <sup>-1</sup> )
2	3 <sub>10</sub> -helix (1650 cm <sup>-1</sup> ) prior to Asp/Glu (1560/1540 cm <sup>-1</sup> )
4	Asp/Glu (1560/1540 cm <sup>-1</sup> ) prior to loop (1683 cm <sup>-1</sup> )
<b>16 – 28 °C</b>	
1	3 <sub>10</sub> -helix (1653 cm <sup>-1</sup> ) prior to random coil (1663 cm <sup>-1</sup> )
2	Random coil (1663 cm <sup>-1</sup> ) prior to Arg (1594/1581 cm <sup>-1</sup> )
3	Arg (1594/1581 cm <sup>-1</sup> ) prior to loop (1682 cm <sup>-1</sup> )
<b>28 – 43 °C</b>	
1	Glu (1544 cm <sup>-1</sup> ) prior to random coil (1668 cm <sup>-1</sup> )
2	random coil (1668 cm <sup>-1</sup> ) prior to Arg (1600/1581 cm <sup>-1</sup> )
3	Arg (1600/1581 cm <sup>-1</sup> ) prior to α-helix (1644 cm <sup>-1</sup> )
4	α-helix (1644 cm <sup>-1</sup> ) prior to loop (1688 cm <sup>-1</sup> )
<b>43 – 58 °C</b>	
1	Glu (1540 cm <sup>-1</sup> ) prior to 3 <sub>10</sub> -helix (1653 cm <sup>-1</sup> )
2	3 <sub>10</sub> -helix (1653 cm <sup>-1</sup> ) prior to random coil (1669 cm <sup>-1</sup> )
3	random coil (1669 cm <sup>-1</sup> ) prior to aggregation (1619 cm <sup>-1</sup> )
4	aggregation (1619 cm <sup>-1</sup> ) prior to Arg (1594/1575 cm <sup>-1</sup> )
5	Arg (1594/1575 cm <sup>-1</sup> ) prior to loop (1684 cm <sup>-1</sup> )
<b>58 – 77 °C</b>	
1	3 <sub>10</sub> -helix (1653 cm <sup>-1</sup> ) prior to Arg (1596/1581 cm <sup>-1</sup> )
2	Arg (1596/1581 cm <sup>-1</sup> ) prior to aggregation (1619 cm <sup>-1</sup> )
3	aggregation (1619 cm <sup>-1</sup> ) prior to loop (1684 cm <sup>-1</sup> )

\*Sequence of spectral intensity changes as temperature is increased.

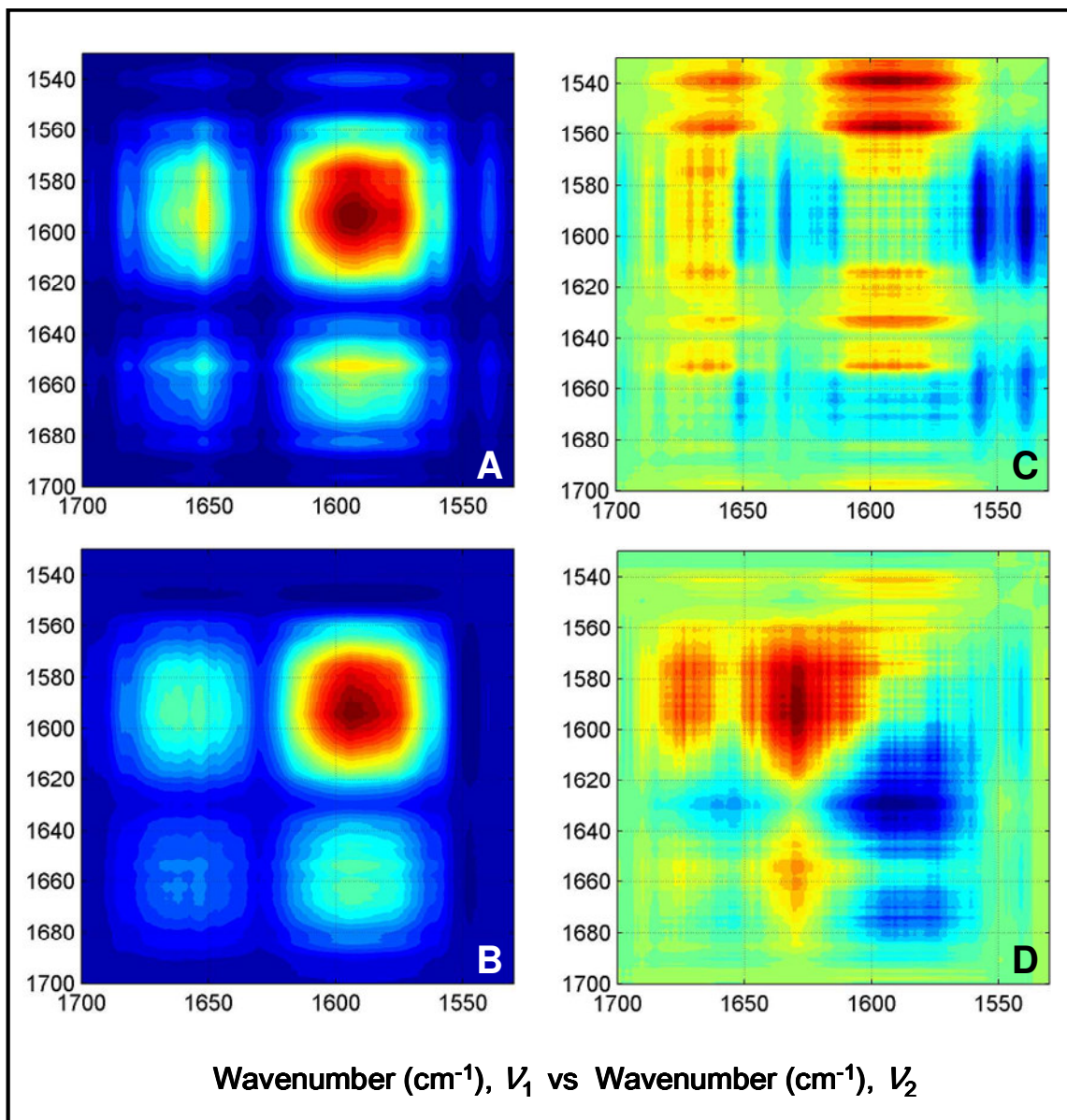


**Figure 31. Two-dimensional correlation analysis from spectral region 1700 – 1500  $\text{cm}^{-1}$  for 2 - 16 °C region ( A, C ) and 16 - 28 °C region ( B, D ) from Hcen2 thermal dependence study.**

(A, B) synchronous plots and (C, D) asynchronous plots of every temperature region.

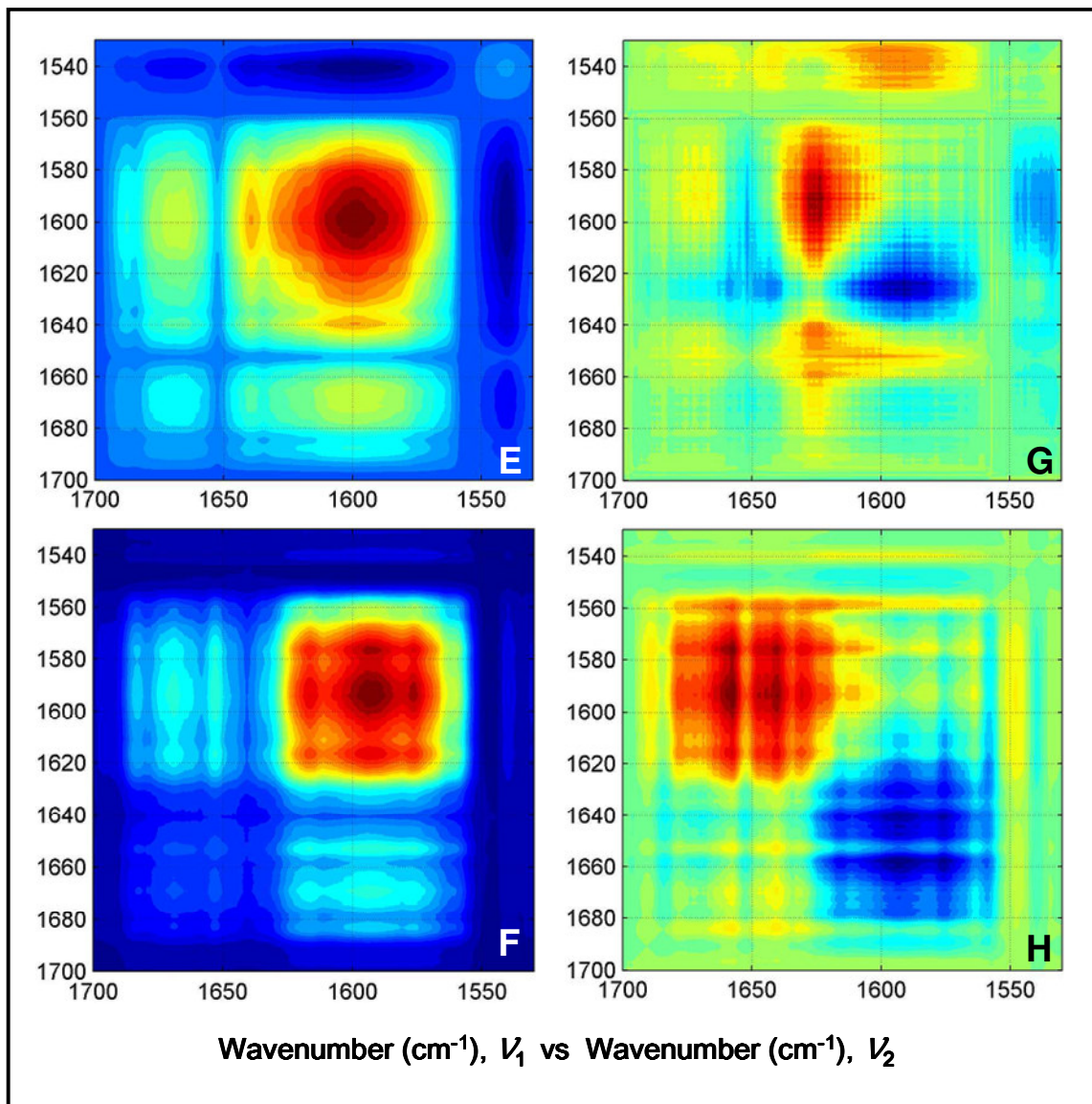


**Figure 32. . Two-dimensional correlation analysis from spectral region 1700 – 1500  $\text{cm}^{-1}$  for 28 – 43 °C region (E, G) and 43 - 58 °C region (F, H) from Hcen2 thermal dependence study.**

(E, F) synchronous plots and (G, H) asynchronous plots of every temperature region.

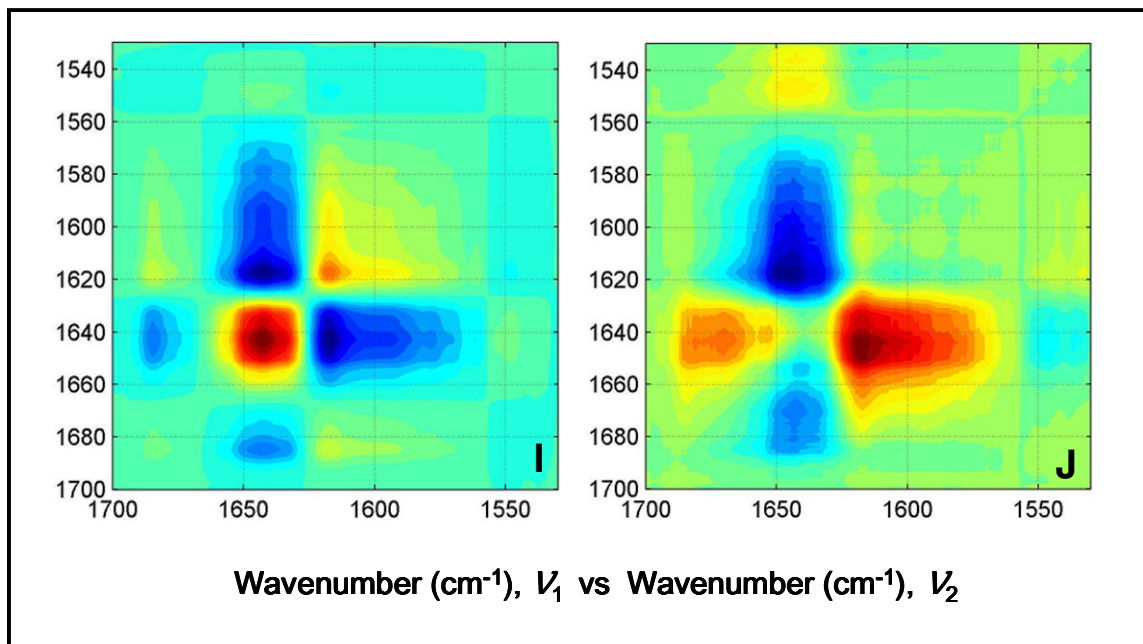


**Figure 33.** Two-dimensional correlation analysis from spectral region 1700 – 1500 cm<sup>-1</sup> for 58 - 77 °C region from Hcen2 thermal dependence study. (I) synchronous and (J) asynchronous plots.

## CHAPTER V

### CONCLUSIONS

Human centrin 1 and Human centrin 2 have more than 80% sequence identity. FT-IR spectroscopy was used to understand the structural and thermal stability differences between Hcen1 and Hcen2. To this end, a thermal perturbation study was performed from 0.5 to 88 °C.

The secondary structure composition for Hcen1 and Hcen2 was determined. A higher  $\alpha$ -helix content was determined for Hcen1 as compared to Hcen2. Additionally, the FT-IR spectroscopic analysis presented herein for Hcen2 is in relative good agreement with the available structural information for this protein (Thompson, et.al. 2006, Martinez-Sanz, et.al. 2006). Differences were observed for the  $\beta$ -sheets composition; this may be due to our results being based on the single component, while the available the structural information is for the Hcen2-peptide complex.

A higher thermal stability was determined for Hcen1 as compared to Hcen2. A pretransition at 1.7 – 4.8 °C was observed for Hcen1 and the onset of the final transition temperature was observed at 80.5 – 84 °C. Unlike Hcen1, Hcen2 was observed to aggregate at a temperature range of 43 – 58 °C.

A complete molecular description was presented for Hcen2 thermal dependence profile which also described the mechanism of aggregation. Consequently, the  $3_{10}$ -helix

(1650  $\text{cm}^{-1}$ ) was more exposed and was responsible for the aggregation of Hcen2 while the  $\alpha$ -helix (1644  $\text{cm}^{-1}$ ) was less exposed and more stable in this protein.

The order of events throughout the thermal perturbation was established where the thermal stability is described for Hcen1 as the follows:

$\alpha$ -helix <  $\beta$ -sheets < glutamate <  $\beta$ -turns

while for Hcen2 the thermal stability is the following:

arginine <  $3_{10}$ -helix < aspartate/glutamate < random coil <  $\alpha$ -helix < aggregation < loops.

FT-IR and two dimensional correlation spectroscopy studies have proven useful in determining the secondary structural composition of Hcen1 and Hcen2, established the relative stability, and provided a description of the dynamic molecular events that occur during thermal perturbation. This method of analysis is therefore sensitive to determining the existence of pretransitions and describing molecular differences observed during a comparative analysis of proteins.

## CHAPTER VI

### FUTURE WORKS

Further investigation of Hcen1 and Hcen2 using differential scanning calorimetry to determine the actual thermal denaturation temperature and the change in heat capacity ( $\Delta C_p$ ) of these proteins will provide their relative stability. Also, the study of centrin complexes with known biologically relevant targets like Sfi1, XPC, and Kar1p using FT-IR and two-dimensional correlation analysis and their crystallization would provide further understanding of the structure function relationship and insight into the molecular level changes by which centrin plays a role in the process of cell division.

## REFERENCES

Araki, M., Masutani, C., Takemura, M., Uchida, A., Sugasawa, K., Kondoh, J., Ohkuma, Y., Hanaoka, F. (2001). Centrosome Protein centrin 2/Caltractin 1 is part of the Xeroderma Pigmentosum Group C Complex That Initiates Global Genome Nucleotide Excision Repair. *J. Biol. Chem.* 276:18665-18672.

Arrondo, J.L., Goñi, F.M. (1999). Structure and Dynamics of membrane proteins as studied by infrared spectroscopy. *Prog. Biophys. Molec. Biol.* 72:367-405.

Arrondo, J.L.R., Muga, A., Castresana, J. and Goñi, F.M. (1993) Quantitative studies of the structure of proteins in solution by fourier-transform infrared spectroscopy. *Prog. Biophys. Molec. Biol.* 59: 23-56.

Azimzadeh, J. and Bornens, M. (2007). Structure and duplication of centrosome. *J. Cell Sci.* 120:2139-2142.

Barth, A. and Zscherp, C. (2002). What vibrations tell about proteins. *Rev. Biophys.* 35:369-430.

Baum, P., Furlong, C. and Byers. (1986). Yeast gene required for spindle pole body duplication: homology of its product with Ca<sup>2+</sup> binding proteins. *Proc. Nat. Acad. Sci. USA.* 83:5512-5516.

Chirgadze, Y.N., Fedorov, O.V., Trushina, N.P. (1975). Estimation of amino acid residue side chain absorption in the infrared spectra of protein solutions in heavy water. *Biopolymers* 14:679-694.

Creighton, T.E. (2002). "Proteins: Structures and Molecular Properties". 2nd Ed. New York: W. H. Freeman and Company.

D'Assoro, A., Lingle, W.L., and Salisbury, J.L. (2002). Centrosome amplification and the development of cancer. *Oncogene* 21:6146-6153.

Doxsey, S. (2001). Re-evaluating centrosome function. *Mol. Cell Biol.* 2:688-698.

Dutcher, S.K., (2001). The tubulin fraternity: Alpha to eta. *Curr. Opin. Cell Biol.* 13: 49-54.

Errabolu, R., Sanders, M. A., and Salisbury, J. L. (1994). Cloning of a cDNA encoding human centrin, an EF-hand protein of centrosomes and mitotic spindle poles. *J. Cell Sci.* 107: 9-16.

Goormaghtigh, E., Raussens, V., Ruyschaert J.M. (1999). Attenuated total reflection infrared spectroscopy of proteins and lipids in biological membranes. *Biochem. Biophys. Acta Rev. Biomem.* 1422:105-85.

Graft, D.K., Pastrana-Rios, B., Venyaminov, S.Y. and Prendergast, F.G. (1997). The Effects of Chain Length and Thermal Denaturation on Helix-Forming Peptides: A Mode-Specific Analysis Using 2D FT-IR. *J. Am. Chem. Soc.* 119:11282-11294.

Hart, P.E., Glantz, J.N., Orth, J.D., Poynter, G.M., and Salisbury, J.L. (1999). Testis-Specific Murine Centrin, Cctn1: Genomic Characterization and Evidence for Retrotransposition of a Gene Encoding a Centrosome Protein. *Genomics* 60:111-120.

Heinz, F. and Mantel, W. (2002). Infrared spectroscopy of proteins. *Encyclopedia Analytical Chemistry*. Ed. John Wiley and Sons Ltd. Pags:1-27.

Hinchcliffe, E. H. and Sluder G. (2001). "It Takes Two to Tango": understanding how centrosome duplication is regulated throughout the cell cycle. *Genes Develop.* 15:1167-1181.

<http://www.rcsb.org/pdb/explore/explore.do?structureId=2GGM>. Accessed on April 2008.

Hu, H., Sheehan, J.H., Chazin, W.J. (2004). The Mode of Action of Centrin Binding of Ca<sup>2+</sup> and a peptide fragment of Kar1p to the C-terminal domain. *J. Biol. Chem.* 279:50895-50903.

Iloro, I. and Pastrana-Rios, B. (2006). Simulation of FT-IR spectra and 2D-COS analysis for the H/D exchange of two related ligands. *J. Mol. Struct.* 799:153-157.

Iloro, I., Narvaez, D., Guillén, N., Camacho, C. M., Guillén, L., Cora, E. and Pastrana-Rios, B. (2008). Kinetics of Hydrogen/Deuterium Exchange of EGFR Ligands. *Biophys. J. BioFAST*. First Published January 16, 2008. doi:10.1529/biophysj.107.125856.

Kilmartin, J.V. (2003). Sfi1 has conserved centrin-binding sites and an essential function in budding yeast spindle body duplication. *J. Cell Biol.* 162:1211-1221.

Kretsinger, R.H., Nockolds, C.E. (1973). Carp muscle calcium-binding protein: II. Structure determination and general description. *J. Biol. Chem.* 248:3313-3326.

Krimm, S. and Bandekar, J. (1986) Vibrational spectroscopy and conformation of peptides, polypeptides and proteins. *Adv. Prot. Chem.* 3: 181-364.

La Terra, S., English, G.N., Hergert, P., McEwen, B.F., Sluder, G., Khodjacob, A. (2005). The novo centriole assembly pathway in HeLa cells: cell cycle progression and centriole assembly/maturation. *J. Cell Biol.* 168:713-722.

Lange, B.MH. (2002). Integration of the centrosome in cell cycle control, stress response and signal transduction pathways. *Curr. Op. Cell Biol.* 14:35-43.

Lee, D.C. and Chapman, D. (1986) Infrared spectroscopic studies of biomembranes and model membranes. *Biosci. Rep.* 6: 235-256.

Levy, Y.Y., Lai, E.Y., Remillard, S.P., Heintzelman, M.B., Fulton, C. (1996). Centrin is a conserved protein that forms diverse associations with centrioles and MTOCs in Naegleria and other organisms. *Cell. Motil. Cytoskel.* 33:298-323.

Lewith-Bentley, A., Réte, S. (2000). EF-hand calcium binding proteins. *Curr. Op. Struct. Biol.* 10:637-643.

Li, S., Sandercock, A.M., Conduit, P., Robinson, C.V., Williams, R.L., Kilmartin, J.V. (2006). Structural role of Sfi1p-centrin filaments in budding yeast spindle pole body duplication. *J. Cell Biol.* 173:867-877.

Liliana del Valle Sosa. 2006. "Structural changes of <sup>13</sup>C-labelled Chlamydomonas centrin and Melittin Upon Complex Formation in the presence of Calcium". *Thesis*.

Lingle, W.L., and Salisbury, J.L. (1999). Altered Centrosome Structure Is Associated with Abnormal Mitoses in Human Breast Tumors. *Am. J. Pathol.* 155: 1941-1951.

Lingle, W.L., Barret, S.L., Negron, V.C., D'Assoro, A., Boeneman, K., Liu, W., Whitehead, C.M., Reynolds, C., and Salisbury, J.L. (2002). Centrosome amplification drives chromosomal instability in breast tumor development. *Proc. Nat. Acad. Sci.* 99:1978-1983.

Lingle, W.L., Lutz, W.H., Ingle, J.N., Maihle, N.J. and Salisbury, J.L. (1998). Centrosome hypertrophy in human breast tumors: Implication for genetic stability and cell polarity. *Proc. Nat. Acad. Sci.* 95:2950-2955.

Lutz, W., Lingle, W.L., McCormick, D., Greenwood, T.M., and Salisbury, J.L. (2001). Phosphorylation of Centring during the Cell Cycle and Its Role in centriole separation preceding centrosome duplication. *J. Biol. Chem.* 276:20774-20780.

Martinez-Sanz, J., Yang, A., Blouquit, Y., Duchambon, P., Asairi, L., Craescu, C.T. (2006). Binding of human centrin 2 to the centrosomal protein hSfi1. *FEBS Journal.* 273:4504-4515.

Meyn, S.M., Seda, C., Cambell, M., Weiss, K.L., Hu, H., Pastrana-Rios, B., Chazin, W.J. (2006). The biochemical effect of Ser167 phosphorylation on Chlamydomonas reinhardtii centrin. *Bioch. Biophys. Res. Comm.* 342:342-348.

Mildred R. Ortiz. 2002. "Attenuated Total Reflectance Fourier Transform Infrared Spectroscopy Study of Chlamydomonas centrin During Hydrogen Deuterium Exchange". *Thesis*.

Nabet, A. and Pezolet, M. (1997). Two-dimensional FT-IR spectroscopy: A powerful method to study the secondary structure of proteins using H-D exchange. *Appl. Spectrosc.* 51:466-469.

Nelson, D. L. and Cox, M. M. (2000). *Lehninger Principles of Biochemistry*, 3rd Edition. New York: Worth Publishers.

Noda, I. and Ozaki, Y. (2004). Two-dimensional Correlation Spectroscopy – Applications in Vibrational and Optical Spectroscopy. West Sussex, England: John Wiley and Sons Ltd.

Noda, I., Dowrey, E., Marcott, C., Story, G.M. and Ozaki, Y. (2000). Generalized two-dimensional correlation spectroscopy. *Appl. Spectr.* 54:236A-248A.

Ortiz, M., Sanoguet, Z., Hu, H., Chazin, W.J., McMurray, C., Salisbury, J.L. and Pastrana-Rios, B. (2005). Dynamics of Hydrogen-Deuterium Exchange in Chlamydomonas Centrin. *Biochemistry.* 44:2409-2418.

Palermo, G.D., Colombero, L.T., Rosenwaks, Z. (1997). The human sperm is responsible for normal syngamy and early embryonic development. *Rev. Reprod.* 2:19-27.

Paoletti, A., Moudjou, M., Paintrand, M., Salisbury, J.L., Bornens, M. (1996). Most of centrin in animal cells is not centrosome-associated and centrosomal centrin is confined to distal lumen of centrioles. *J. Cell Sci.* 109:3089-3102.

Pastrana-Rios, B. (2001). Mechanism of Unfolding of a Model Helical Peptide. *Biochemistry.* 40: 9074-9081.

Pastrana-Rios, B. (2006). Simulation of FT-IR spectra and 2D-COS analysis for the thermal perturbation of apo-centrin. *J. Mol. Struct.* 799:163-167.

Pastrana-Rios, B. Ocaña, W., Rios, M., Vargas, G. L., Ysa, G., Poynter G., Tapia, J. and Salisbury, J.L. (2002). Centrin: Its Secondary Structure in the presence and absence of cations. *Biochemistry.* 41:6911-6919.

Popescu, A., Miron, S., Blouquit, Y., Duchambon, P., Christova, P., and Craescu, C. T. (2003) Xeroderma Pigmentosum Group C Protein Possesses a High Affinity Binding Site to Human Centrin 2 and Calmodulin. *J. Biol. Chem.* 278:40252-40261.

Raussens, V., Ruyschaert, J.M and Goormaghtigh, E. (2004). Analysis of 1H/2H exchange kinetics using model infrared spectra. *Appl. Spectrosc.* 58:68-82.

Salisbury, J. L. (1995). Centrin, centrosomes, and mitotic spindle poles. *Curr. Op. Cell Biol.* 7:39-45.

Salisbury, J. L., Whitehead, C. M., Lingle, W. L. and Barret, S. L. (1999). Centrosomes and Cancer. *Biol. Cell.* 91:451-460.

Salisbury, J., Suino, K., Busby, R., and Springett, M. (2002). Centrin-2 is required for centriole duplication in mammalian cells. *Curr. Biol.* 12: 1287-1292.

Salisbury, J.L., Baron, A., Surek, B., Melkonian, M. (1984). Striated flagellar roots: isolation and partial characterization of a calcium-modulated contractile organelle. *J. Cell Biol.* 99:962-970.

Sanoguet, Z. Cambell, M., Ramos, S., Seda, C., Pérez Moreno, L. and Pastrana-Rios, B. (2006). Effects of Phosphorylation in Chlamydomonas Centrin Ser 167. *Calcium Binding Proteins.* 1:108-114.

Schiebel, E. and Bornens, M., (1995). In search of a function of centrins. *Trends Cell Biol.* 5: 197-201.

Sheehan, J.H., Bunick, C.G., Hu, H., Fagan, P., Meyn, S.M., Chazin, W.J. (2006). Structure of N-terminal Calcium Sensor Domain of Centrin Reveals the Biochemical Basis for Domain-specific Function. *J. Biol. Chem.* 281:2876-2881.

Snell, W.J., Pan, J., and Wang, Q. (2004). Cilia and flagella revealed; from flagellar assembly in *Chlamydomonas* to human obesity disorders. *Cell* 117:693-697.

Solomon, Berg and Martin (2002), "Biology", 5th Ed. Harcourt College Publishers

Thompson, J.R., Ryan, Z. C., Salisbury, J.L., Kumar, R. (2006). The structure of human centrin 2 –Xeroderma Pigmentosum Group C protein complex. *J. Biol. Chem.* 281:18746-18752.

Vigano, C., Smeyers, M., Raussens, V., Scheirlinckx, F., Ruyschaert J.M., and Goormaghtigh, E. (2004). Hydrogen- deuterium exchange in membrane proteins monitored by IR spectroscopy: A new tool to resolve protein structure and dynamics. *Biopolymers* 74:19-26.

Wanda Ocaña. 2002. "Ca<sup>+2</sup>/Mg<sup>+2</sup> Binding Characteristics of *Chlamydomonas* centrin domains". *Thesis*.

Weber, C., Lee, V., Chazin, W. Huang, B. (1994). High level expression in *Escherichia coli* and characterization of the EF-hand calcium binding protein caltractin. *J. Biol. Chem.* 76:383-388.

Weich, H., Geier, B.M., Paschke, T., Spang, A., Grein, J., Steinkotter, J., Melkonian, M., and Schiebel, E. (1996). Characterization of the Green Algae, Yeast and Human centrins. *J. Biol. Chem.* 271:22453-22461.

Wolfrum, U., Giessl, A., and Pulvermüller, A. (2002). Centrins, a novel group of Ca<sup>2+</sup> binding proteins in vertebrate photoreceptor cells, in *Photoreceptors and Calcium* (Baehr, W., and Palczewski, K., Eds.) pp 154-178, New York: Kluwer Academic/Plenum Publishers,

Yang, A., Miron, S., Duchambon, P., Assairi, L., Blouquit, Y., Craescu, C.T. (2006a). The N-Terminal Domain of Human Centrin 2 Has a Closed Structure, Binds Calcium with a Very Low Affinity, and Plays a Role in the Protein Self-Assembly. *Biochemistry* 45:880-889.